

SUBMISSION TO
JOURNAL OF GEOMECHANICS FOR ENERGY AND THE ENVIRONMENT
SPECIAL ISSUE ON 'LOW CARBON GEOTECHNICS'

DATE:

Written: June 2020

Revised March 2020

TITLE:

Evaluation of instruments for monitoring the soil-plant continuum

AUTHORS:

Roberta Dainese^{1,2,3}

Bruna de Carvalho Faria Lima Lopes¹

Thierry Fourcaud²

Alessandro Tarantino¹

AFFILIATION:

¹ Department of Civil and Environmental Engineering, University of Strathclyde, Glasgow, UK

² CIRAD, UMR AMAP, F-34398 Montpellier, France

³ AMAP, Univ Montpellier, CIRAD, CNRS, INRAE, IRD, Montpellier, France

CORRESPONDING AUTHOR:

Dr Roberta Dainese

Department of Civil and Environmental Engineering

University of Strathclyde

James Weir Building - Level 5

75 Montrose Street - Glasgow G1 1XJ, Scotland, UK

E-mail: roberta.dainese.rd@gmail.com

KEYWORDS

High-Capacity Tensiometer, Pressure Chamber, Thermocouple Psychrometer, Xylem water tension, Soil water tension, Time Domain Reflectometry, Electrical Resistivity Tomography

1 **Evaluation of instruments for monitoring the soil-plant**
2 **continuum**

3 *R. Dainese, B. de C. F. L. Lopes, T. Fourcaud, and A. Tarantino*
4

5 **Abstract**

6 The response of the shallow portion of the ground (vadose zone) and of earth structures is
7 affected by the interaction with the atmosphere. Very frequently, the ground surface is
8 covered by vegetation and, as a result, transpiration plays a major role in ground-
9 atmosphere interaction. The soil and the plant form a continuous hydraulic system that
10 needs to be characterised to model the ‘boundary condition’ of the geotechnical water
11 flow problem. Water flow in soil and plant takes place because of gradients in hydraulic
12 head triggered by the water tension (negative water pressure) generated in the leaf stomata.
13 To study the response of the soil-plant continuum, water tension needs to be measured not
14 only in the soil but also in the plant (in addition to the water content in the soil). This paper
15 first evaluates three instruments that can be used to measure xylem water tension, i.e. the
16 High-Capacity Tensiometer (HCT) and the Thermocouple Psychrometer (TP) for
17 continuous non-destructive measurement on the stem, and the Pressure Chamber (PC) for
18 discontinuous destructive measurement on the leaves. Experimental procedures are
19 presented and critically discussed, including data quality control and instrument
20 calibration, accuracy, and precision. The performance of these three instruments is
21 evaluated in terms of measurement precision and measurement accuracy via cross-
22 validation. The paper then addresses the problem of monitoring soil suction (pore-water

23 tension) and water content using a second generation profile probe (fully encapsulated)
24 and the use of Electrical Resistivity Tomography (ERT) for coarse characterisation of
25 water content spatial distribution to support the design of spatial configuration of suction
26 and water content sensors.

27

28 **1 Introduction**

29 The response of the shallow portion of the ground (vadose zone) and of earth structures is
30 affected by the interaction with the atmosphere. Rainwater infiltration and
31 evapotranspiration cause settlement and heave of shallow foundations and embankments
32 and control the stability of man-made and natural slopes. The ground surface is very
33 frequently covered by vegetation, which therefore represents the interface modulating the
34 interaction between the ground and the atmosphere.

35 Vegetation affects directly the ground water regime in the vadose zone via
36 transpiration. This is the process of water movement taking place from the soil through
37 the plant up to the leaves, where water eventually evaporates through the stomata, and
38 plays a major role in the mechanisms of water removal by the atmosphere. The soil and
39 the plant form a continuous hydraulic system (Philip, 1966) which needs to be
40 characterised to model the ‘hydraulic boundary condition’ of the water flow problem.

41 Understanding and modelling the mechanisms through which vegetation mediates the
42 interaction between ground and atmosphere is key to assess climate-related geotechnical
43 geohazards. These include rainfall-induced landslides (Gonzalez-Ollauri & Mickovski;
44 2017), low-rise building damage associated with drought-induced foundation subsidence
45 (Deakin, 2005; Corti et al. 2011, Toll et al. 2012), and flood-induced instability of stream
46 banks (Pollen et al. 2004). Vegetation can also be viewed as a ‘technology’ to mitigate
47 diffuse hazard such as diffuse shallow landsliding (Alcántara-Ayala et al. 2006, Dolidon
48 et al. 2009). Pagano et al. (2018) have shown that vegetation can lower the degree of
49 saturation during the dry period more efficiently than the bare soil and this reduces the

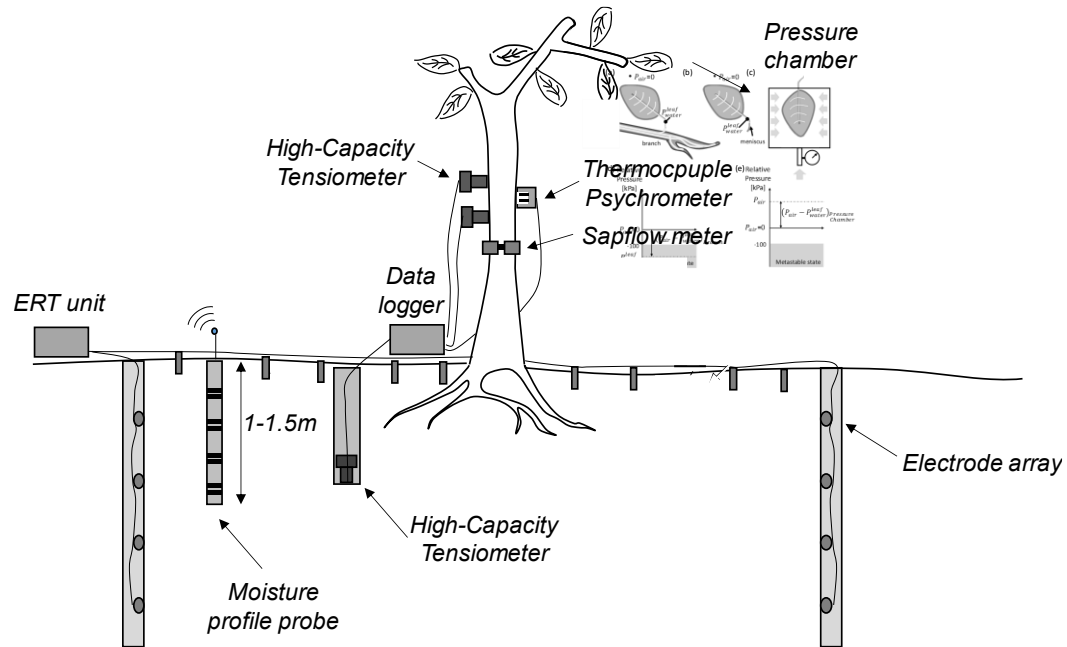
50 pore-water pressure build-up during rainfall events thus improving the factor of safety of
51 slopes.

52 The hydrological response of the soil-plant continuum is difficult to investigate in the
53 laboratory. An experiment representative of field conditions is difficult to reproduce at the
54 laboratory scale because of the size of plants, diversity of plant species, and the complex
55 microstructure of the rhizosphere soil deriving from long-standing bio-chemical
56 processes. The study of the bio-mediated interaction between the ground and the
57 atmosphere therefore requires an open-air laboratory approach, i.e. it is the laboratory to
58 be moved to the field and not vice versa.

59 This paper presents a monitoring concept for the soil-plant continuum (Figure 1) and
60 includes instruments to monitor the water status in the plant and the ground. This system
61 should be complemented by a weather station to monitor atmospheric variables and the
62 reader can refer to the literature for discussion about this component of the soil-plant
63 continuum monitoring (e.g. WMO, 2018).

64 The main challenges faced by geotechnical researchers and practitioners with respect
65 to traditional geotechnical monitoring of the vadose zone are represented by the
66 measurement of the water potential and flow rate of xylem water. The paper therefore
67 mainly focuses on the measurement of xylem water tension by presenting and comparing
68 the measurements by three different techniques, i.e. High-Capacity Tensiometer,
69 Thermocouple Psychrometer, and Pressure Chamber. The paper therefore focuses on the
70 monitoring soil matric suction using the High-Capacity Tensiometer and soil water
71 content using a profile probe of second generation, which is fully encapsulated and does

72 not require the pre-installation of a casing. The paper finally discusses the use of Electrical
 73 Resistivity Tomography (ERT) to guide the design of the installation of ‘local’ suction
 74 and water content sensors.



75

76 **Figure 1.** Soil-Plant monitoring system concept

77 **2 Measurement on plant**

78 **2.1 HCT for xylem water potential measurement**

79 The High-Capacity Tensiometer (HCT) is composed of an integral strain gauge, a
 80 diaphragm 0.4 mm thick and a ceramic filter with nominal air-entry value of 1.5 MPa
 81 (Tarantino & Mongiovi, 2002). The working principle and the experimental procedures
 82 adopted i) to saturate the porous ceramic filter and i) to check its saturation prior to and
 83 after the measurement are discussed in Tarantino (2004) whereas details of HCT

84 installation on the stem are provided in Dainese et al (2020a). The measurement of xylem
85 water potential using the HCT has been validated by Dainese & Tarantino (2020) and
86 Dainese et al. (2020b) by comparison with Pressure Chamber and Thermocouple
87 Psychrometer on different trees and saplings. The advantage of the HCT with respect to
88 the Thermocouple Psychrometer, which is the other instrument available for continuous
89 monitoring of xylem water potential, is that its measurement is not affected by the solute
90 concentration of the sap (osmotic suction) and that the same probe can be used to monitor
91 both soil and plant. This paper discusses in detail the experimental procedures to enable
92 accurate measurement of xylem water tension.

93 An example of measurement of xylem water pressure by the HCTs is shown in Figure
94 2 for the case of a Cherry sapling (*Bigarreau burlat*). The measurement lasted 30 days
95 and two different sets of HCTs were used. HCT 5 and HCT6 were installed for the first
96 15 days (positioned 30cm and 20cm respectively above the soil) and then removed after
97 cavitation. HCT2 and HCT4 were installed on day 16 (positioned 11.5cm and 25cm
98 respectively above the soil) and were kept in place for the following 13 days. As water in
99 the xylem flows upward, the higher HCT should record in principle a lower xylem water
100 pressure than the lower HCT. This differential is not recorded for the pair HCT2 and
101 HCT4, which indicates that the small difference between the two HCTs is due to local
102 variations of xylem water pressure.

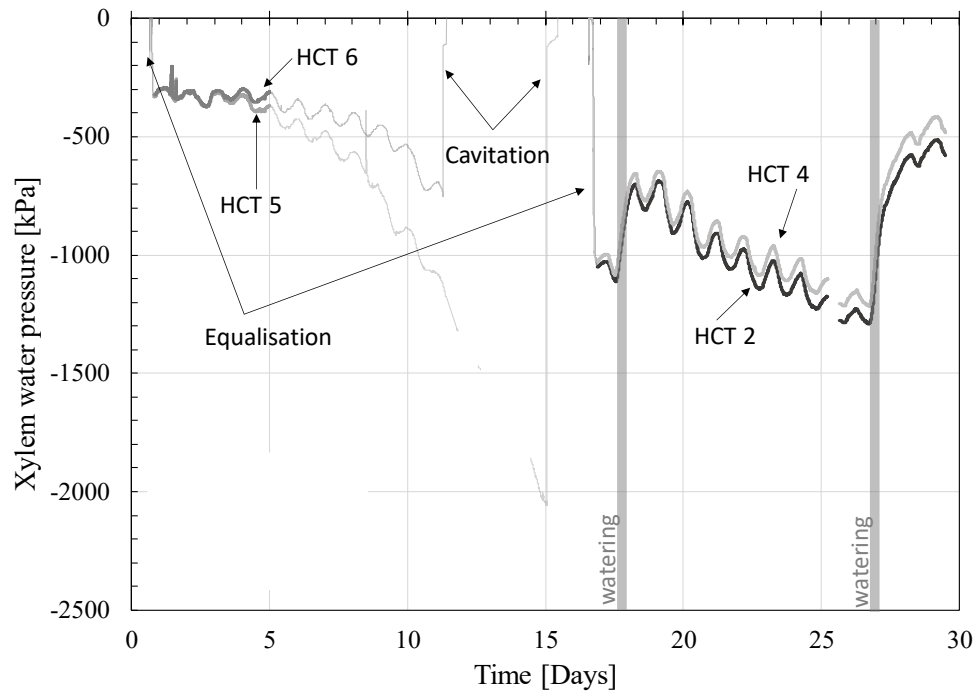
103 . HCT 6 cavitated at day 11 at a water pressure of -750 kPa while HCT 5 cavitated at
104 day 15 at a water pressure of -2055 kPa. Both HCTs recorded a post-cavitation
105 measurement close to -100 kPa (-111 kPa and -118 kPa for HCT6 and HCT 5

106 respectively). Cavitation in Figure 2 appears as a vertical straight line interrupting abruptly
107 the measurement (day 11 and day 15 respectively). They then returned to a value close to
108 zero when the tensiometers were placed into free water. The detail of the cavitation
109 process is shown in Figure 3.a.

110 The very steep curves on day 1 and day 17 are associated with the hydraulic
111 equilibration between the instrument and the xylem. The saturated paste needs to lose
112 water to the xylem until equilibrium is achieved (Figure 3.b). The HCT readings during
113 the equilibration are therefore not representative of the water status of the plant.

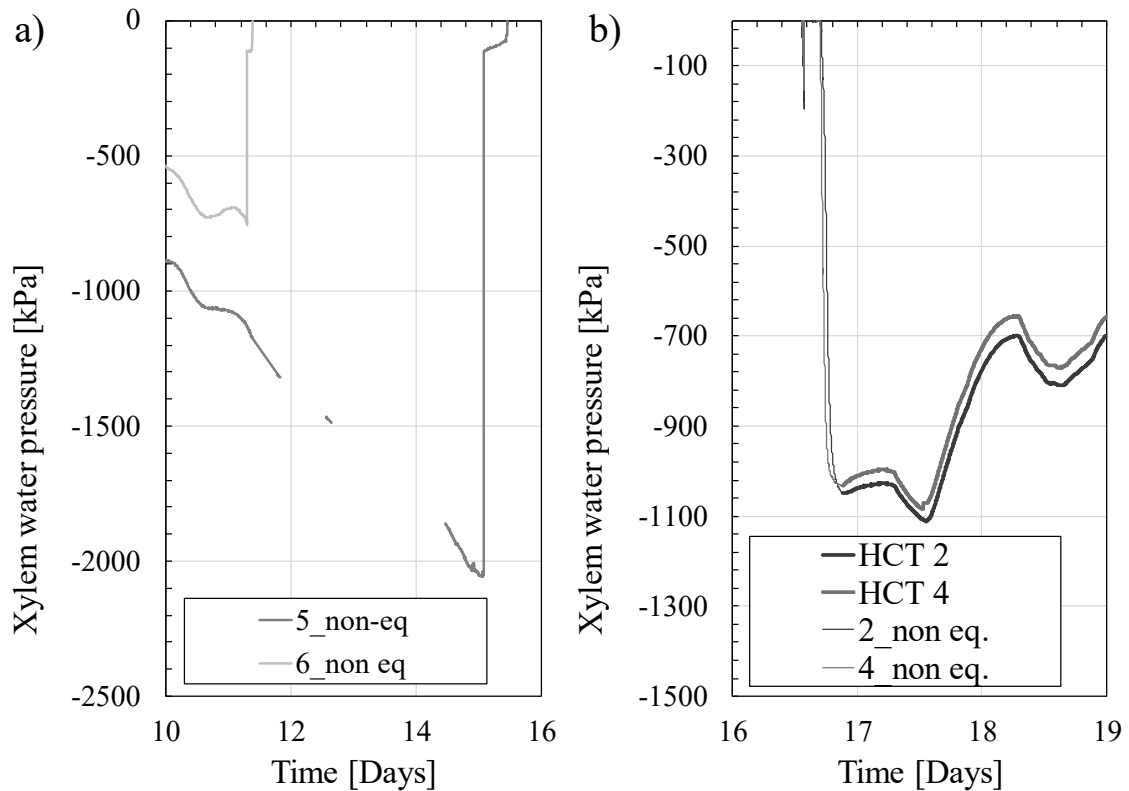
114 The HCT measurement was considered to be valid during the first 5 days since the
115 readings of the two HCTs were overlapping. On the other hand, the measurements of
116 HCT5 and HCT6 were considered to not be valid after day 5 since the readings diverged
117 more than 50 kPa. The divergence between the two readings could be attributed to an
118 ongoing cavitation process in HCT5 or a change in xylem water pressure at the measuring
119 site of either HCT5 or HCT6. Another possible reason is the healing processes occurring
120 at the measuring site (Lev-Yadun, 2011) already observed in the thermocouple
121 psychrometer (Dixon & Downey, 2015). Since it is not possible to identify, between the
122 two tensiometers installed on the plant, the one that generated the faulty measurement,
123 the measurements of both instruments are discarded. On the other hand, the measurements
124 of the two tensiometers installed on day 16, HCT2 and HCT4 respectively, were always
125 overlapping and their measurement was then considered valid. The valid measurements
126 of xylem water pressure via HCTs are reported in Figure 2 with thick curves while the
127 readings to be considered invalid are represented by thin curves.

128 Figure 2 shows that if only one HCT was installed on the stem between days 5 and 15,
129 its measurement would have appeared correct because readings exhibit daily fluctuations
130 due to the day/night cycles. The simultaneous installation of two HCTs is therefore
131 essential to validate the measurement.



132

133 **Figure 2.** Measurement of HCT on the cherry sapling. The thick lines represent the measurement
134 in hydraulic equilibrium with the xylem, the fine lines represent the non-valid measurement of
135 xylem water pressure.



136

137 **Figure 3.** Details of a) Cavitation of HCT 5 and HCT 6. b) installation and equilibration (thin
 138 lines) of HCT 2 and HCT 4.

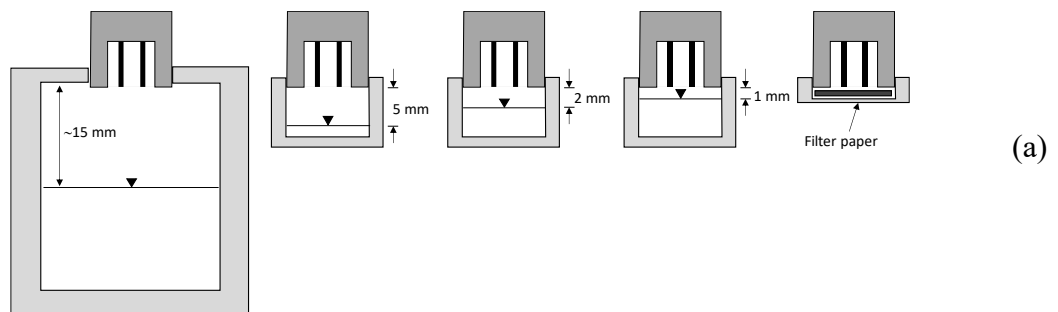
139 2.2 Thermocouple Psychrometer

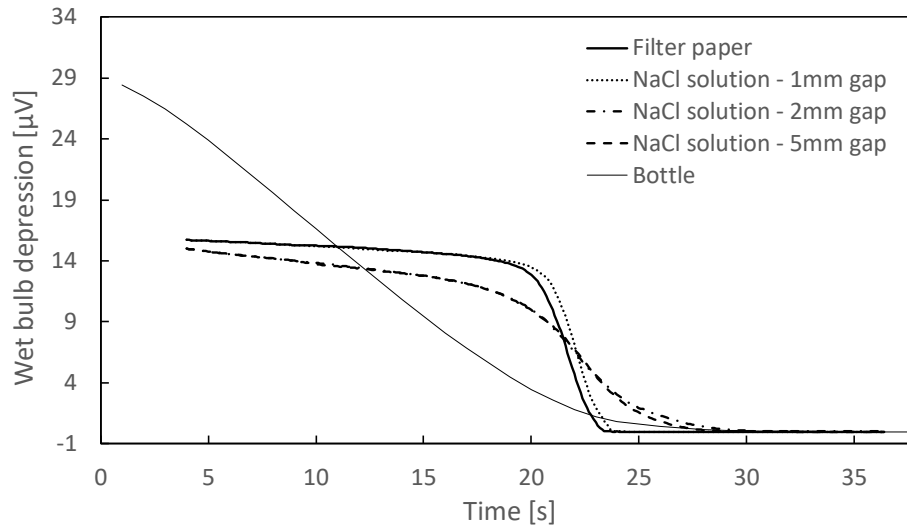
140 The Thermocouple Psychrometer (TP) considered in this work is produced by ICT
 141 international (PSY1 Stem Psychrometer). The psychrometer measures the relative
 142 humidity of the air in equilibrium with the xylem water, which is then converted to xylem
 143 water pressure via the psychrometric law. Details of the TP working principle are provided
 144 in Dixon & Downey (2015).

145 The thermocouples of the psychrometer are handmade and therefore need to be
 146 calibrated individually. The manufacturer suggests to calibrate the sensor by using filter

147 paper soaked in NaCl solution. The filter paper can potentially introduce a bias due to the
148 menisci that may form at the filter paper-air interface and the matric component of suction
149 generated thereof. To investigate this potential effect three calibration systems were
150 considered: i) a bottle filled with NaCl solution with about 15 mm gap between the liquid
151 surface and the thermocouple , ii) a small cap filled with NaCl solution with various air
152 gaps (5 mm, 2 mm, and 1 mm), and iii) a filter paper soaked with NaCl solution (Figure
153 4.a**Error! Reference source not found.**).

154 The decay of the electrical potential versus time for the 5 setups in Figure 4.a is shown
155 in Figure 4.b. The signal at equilibrium (achieved when the signal did not change any
156 longer over time) should in principle not be affected by the air gap (i.e. the distance
157 between the sensor and the evaporating surface). Nonetheless, the experimental data
158 showed the opposite possibly due to larger thermal gradients occurring in the larger gaps.
159 However, the signal tends to converge when the air gap becomes sufficiently small (1mm
160 above free solution or less than 1mm above filter paper). The results of Figure 4.b was
161 taken as an evidence that calibration using the filter paper is appropriate and the
162 thermocouple was therefore calibrated using this calibration system.





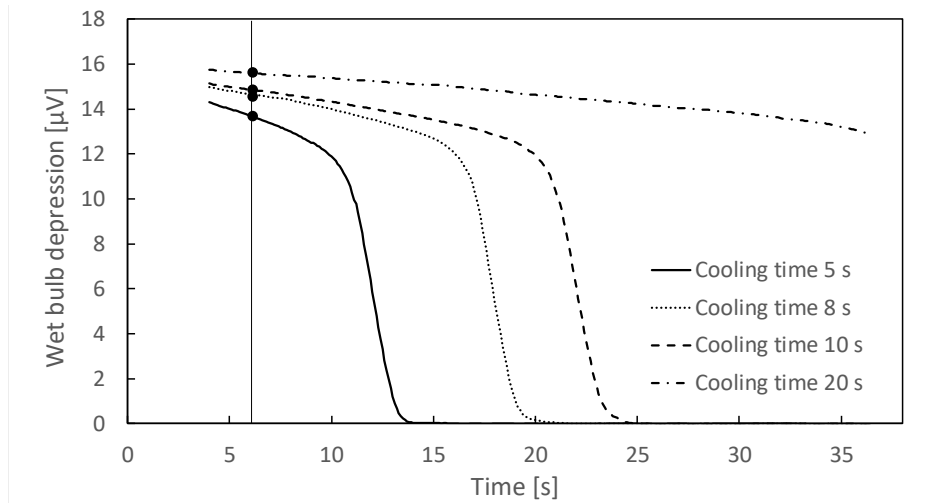
(b)

163 **Figure 4.** Calibration of Thermocouple Psychrometer by exposure to 1.0 mol NaCl solution (-4.55
 164 MPa. (a) Calibration setups. (b) Effect of air gap (Cooling time = 10 sec except bottle where
 165 cooling time was set to 20 sec)

166 The thermocouple signal depends on the Cooling Time, i.e. the time whereby the
 167 current is circulated in the thermocouple to cool the thermocouple junction and cause the
 168 condensation of a water drop. The effect of the cooling time on the electrical signal is
 169 shown in Figure 5. The longer the current is circulated through the thermocouple, the
 170 larger is the drop condensing on the junction and the higher is the thermal inertia delaying
 171 the drop in differential temperature and, hence, electrical potential.

172 It is worth noticing that the cooling time affects the signal but not the tangent at the
 173 inflection point, which remains the same regardless of the cooling time. As a result,
 174 calibration curves relating the water potential to the electrical response should be in
 175 principle built using the slope of the tangent at the inflection point. However, the ranges
 176 of start acquisition time and length of the acquisition window that can be set up using this

177 particular instrument do not always allow detecting the entire decay curve. It follows that
178 another characteristic of the electrical signal should be adopted to build the calibration
179 curve.



180

181 **Figure 5.** Effect of cooling time (CT) on the signal recorded by the Thermocouple Psychrometer
182 (exposed to NaCl solution of -4.55 MPa water potential (NaCl 1.0 mol)

183 The manufacturer suggests to detect the electrical signal at a given time, which is
184 referred to as Wait Time in the PSY1 manual (Dixon & Downey, 2015). However, Figure
185 5 shows that the electrical signal at given time (e.g. 6 s) depends on the cooling time. As
186 a result, the decay curve returned by the instrument was investigated for two different
187 cooling times (5s and 8s respectively). For each cooling time, two different acquisition
188 windows were considered, 4-36 s and 13-45 s respectively, to enable a Wait Time of either
189 6 s (4+2 s) or 15 s (13+2 s) respectively.

190 Figure 6 presents the decay curves derived for two cooling times and two different
191 acquisition windows recorded by exposing the thermocouple to NaCl solutions having

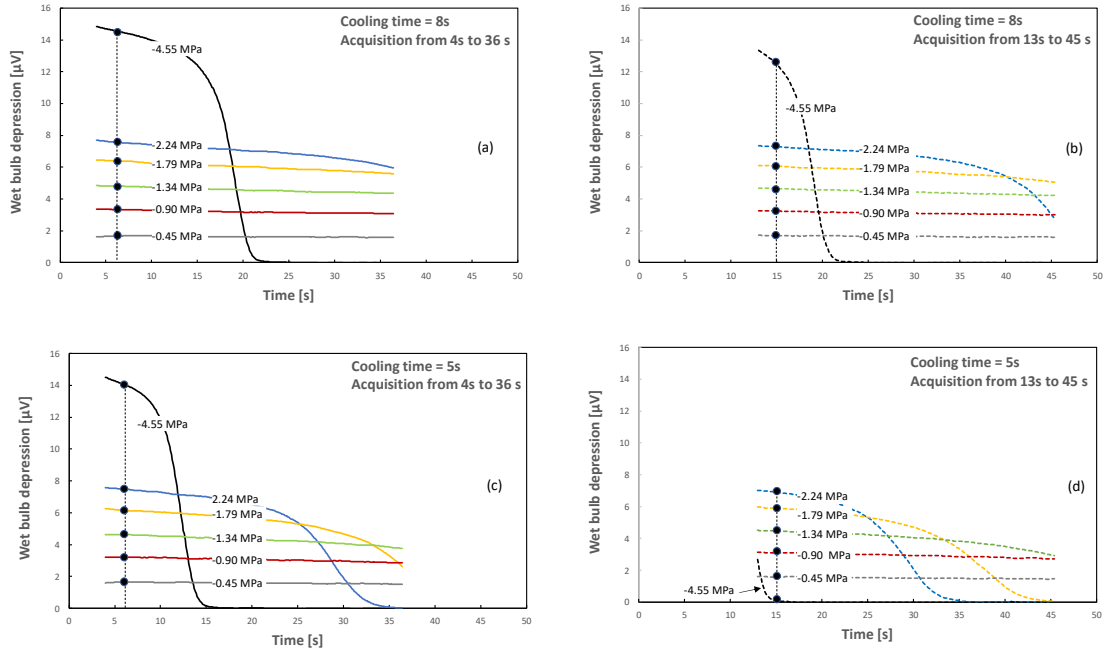
192 water potential ranging from -0.45 to -4.55 MPa (0.1 to 1 molality). The lower the water
193 potential (lower relative humidity), the lower is the temperature required to cause water
194 drop condensation and, hence, the higher is the initial voltage differential. At the same
195 time, the lower the water potential (i.e. the lower is the relative humidity), the faster is the
196 water drop evaporation and, hence the decay in voltage differential.

197 Figure 6.a and Figure 6.b show the decay curves for 8s Cooling Time and the two
198 different acquisition windows. In both cases, the signal recorded at the Wait Time
199 decreases monotonically as water potential increased from -4.55 MPa to -0.5 MPa.

200 Figure 6.c and Figure 6.d show the decay curves for 5s cooling time and the two
201 different acquisition windows. It is worth noticing that the signal at -4.55 MPa for the
202 Wait Time of 15s decays faster than the Wait Time itself. As a result, the signal recorded
203 at the Wait Time at higher lower water potentials becomes suddenly the lowest rather than
204 the highest. The correlation between voltage differential and water potential therefore
205 loses monotonicity. A relatively short Wait Time therefore need to be selected to avoid a
206 non-unique relationship between water potential and voltage differential recorded at the
207 Wait Time.

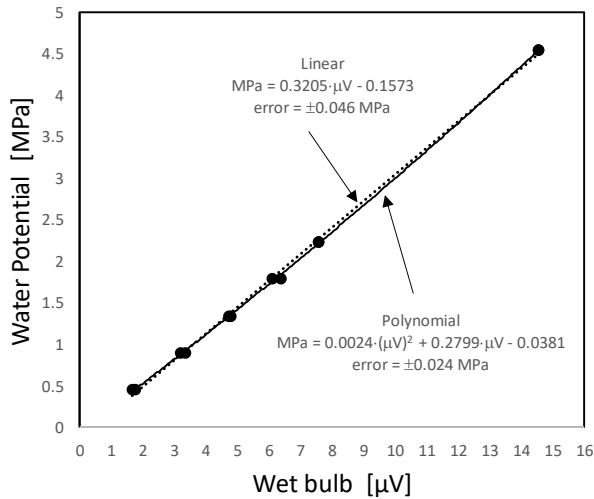
208 The calibration curve derived from an 'loading-unloading' cycle with Cooling Time =
209 8 s and Wait Time = 6 s is shown in Figure 7. The calibration is essentially linear although
210 accuracy can be slightly improved by adopting a polynomial of the second order (standard
211 deviation of the error reduced to ± 0.024 MPa from the value of ± 0.046 MPa associated
212 with the linear calibration).

213



214

215 **Figure 6.** Effect of cooling time (CT) and Start Acquisition Time (SAT) on the signal recorded by
 216 the Thermocouple Psychrometer exposed to NaCl solutions of different water potential. (a) CT=8s
 217 and SAT = 4s. (b) CT=8s and SAT = 13s. (c) CT=5s and SAT = 4s. (d) CT=5s and SAT = 13s.



218

219 **Figure 7.** Calibration curve derived from a 'loading-unloading' cycle and Cooling Time = 6s and
220 Wait Time = 6 s

221 **2.3 Pressure Chamber**

222 The working principle of the Pressure Chamber (PC) is analogous to the axis-translation
223 technique used in soil testing (Marinho et al., 2008) and is discussed in detail in
224 Scholander et al. (1965) and Boyer (1967). The measurement of the PC is discontinuous
225 and destructive; the frequency of the readings is therefore conditioned by the manpower
226 and the sampling leaves available. The PC is a commonly used and trusted technique in
227 plant science to measure the 'xylem' matric water pressure in plants and has been often
228 used as a benchmark to validate other techniques (Brown and Tanner, 1981; Turner et al.,
229 1984; Balling, & Zimmermann, 1990).

230 The PMS 1515D Scholander Pressure Chamber (PMS Instrument, 2018) was used in this
231 work for the xylem water pressure measurement **Error! Reference source not found..**

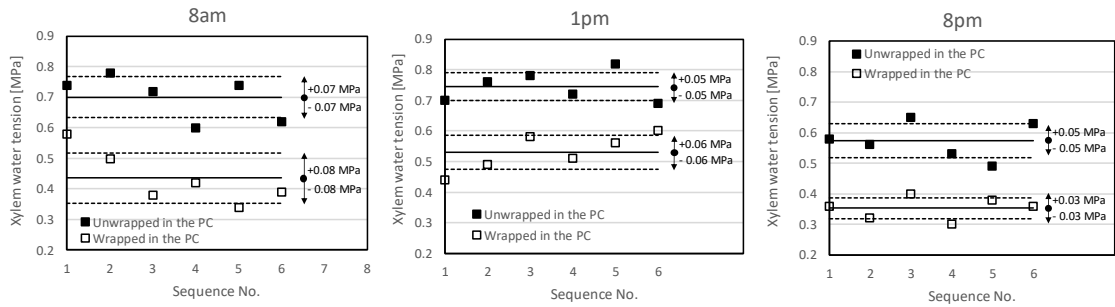
232 Leaves were initially wrapped in aluminium foil for at least 2h. Leaf wrapping stops
233 transpiration and allows water in the leaf to equilibrate with the branch. As a result, the
234 water pressure recorded in the leaf is assumed to coincide with the water pressure in the
235 branch at the base of the petiole.

236 The leaf was then excised with a sharp blade and promptly inserted into the pressure
237 chamber where air was gradually pressurised until a flat meniscus formed at the end of
238 the excised petiole (Meron et al., 1987). The air pressure in the chamber recorded when a

239 flat meniscus appeared at the excised petiole surface is assumed to be equal to the negative
240 water pressure in the leaf before excision.

241 The precision of the measurement using the Pressure Chamber is affected by the intrinsic
242 variability between leaves and also by the subjective judgment made by the operator about
243 the appearance of a water film at the surface of the excised petiole. To investigate the
244 measurement precision, leaves were cut from a tree on the campus of the University of
245 Strathclyde at three different times in a day, 8am, 1pm, and 8pm respectively (sunrise
246 4:45am and sunset on 9.21pm on 26 May). Two sets of six leaves were placed in the
247 pressure chamber, the first set without removing the aluminium foil used to wrap the leaf
248 'in situ' before excision and the second set by removing the aluminium foil just before
249 placing the leaf in the pressure chamber. Figure 8 shows that:

- 250 1) the precision of the measurements is satisfactory, ranging from 0.03 to 0.08 MPa in
251 terms of standard deviation;
- 252 2) the average xylem water tension is consistently higher during the day (8am and 1pm)
253 and lower when approaching sunset (8pm)
- 254 3) removing the aluminium foil just before the insertion in the pressure chamber leads to
255 an overestimation of the xylem water tension possibly because of some evaporation
256 occurring over the time the leaf remains exposed to the air.



257

258 **Figure 8.** Precision of Pressure Chamber measurement and effect of maintaining or removing the
 259 aluminium foil wrapping the leaf in the pressure chamber (standard deviation of the error is
 260 reported next to each set of measurements) .

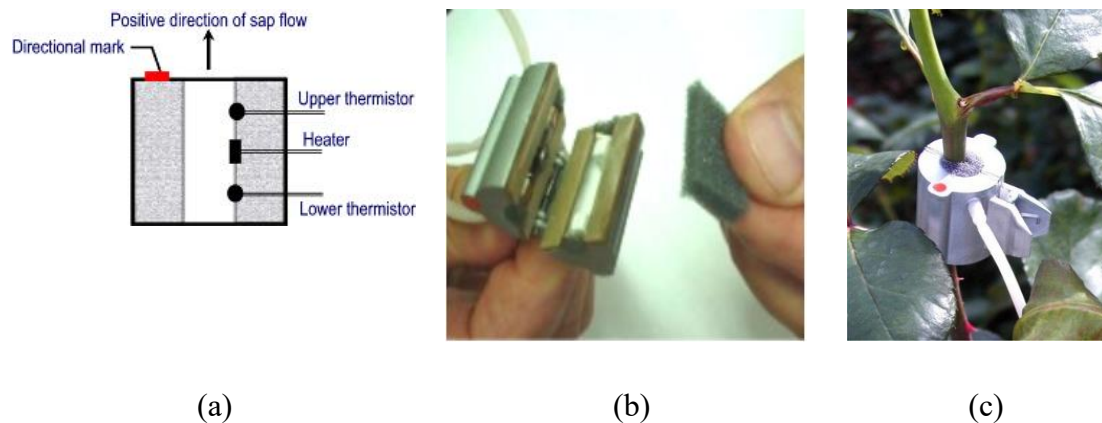
261 **2.4 Stemflow meter**

262 Traditional sensors used to measure the flux of sap are based on the design of the Granier's
 263 Thermal Dissipation Probe (TDP). In the original version two probes are inserted within
 264 the trunk, at a distance of 10-15 cm on the vertical axis. Each probe contains a heating
 265 element and a thermocouple. During the measurement, the higher probe (downstream to
 266 the sap flux) is heated with a constant voltage, while the lower probe (upstream) is used
 267 as a reference of the wood temperature. The difference in temperature registered by the
 268 two probes, measured in terms of difference in voltage, is influenced by the heat
 269 dissipation effect of sap flow in the vicinity of the heated probe (Lu et al. 2004). The sap
 270 flow sensor used during this study is a modification of the TDP, where the heater and the
 271 two bead thermistors are placed within a heat-insulating hollow cylinder, and no drilling
 272 and installation of the stem is required (Anon., n.d.). The sap flow sensor used is produced

273 by Edaphic Scientific and it is suitable for the application on small stems (1-5 mm and 4-
274 10 mm depending on the model used).

275 The simplified design of the probe allows a quick installation by simply clamping the
276 two parts of the probe around the selected twig (Figure 9). The manufacturer suggests
277 isolating the measuring site with aluminium foil to avoid thermal disturbances. The output
278 generated by the sensor is a voltage signal.

279



280 **Figure 9.** Stemflow meter. (a) Working principle. (b) Clamping system (c) Installation on stem.

281 2.5 Comparing techniques for plant water status measurement

282 2.5.1 Stem-flow versus High-Capacity Tensiometer

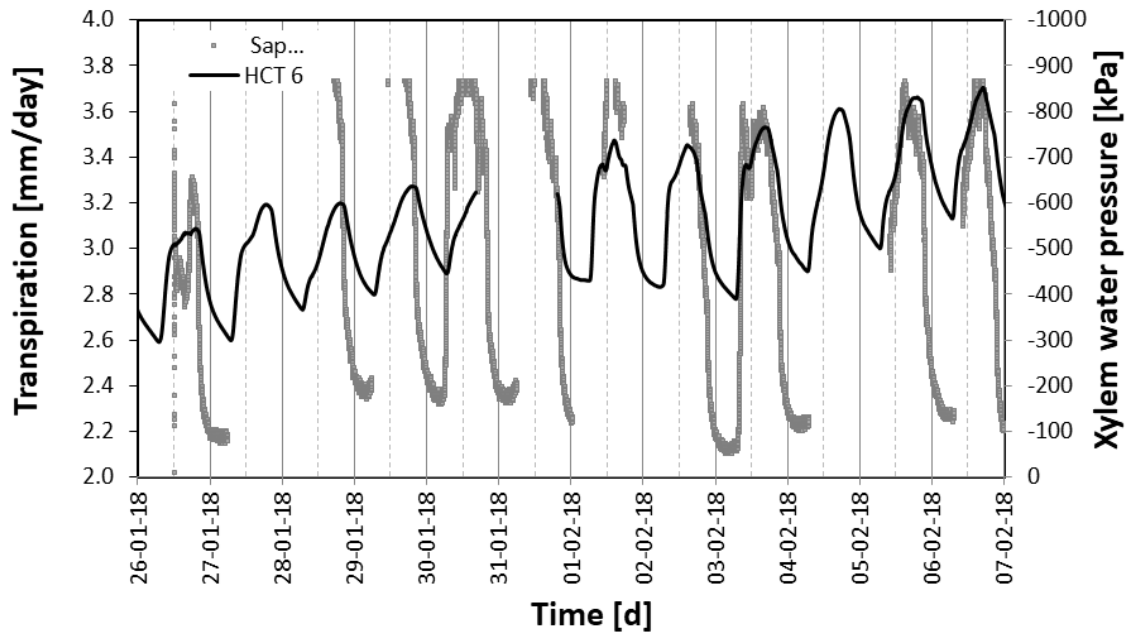
283 The stemflow meter and HCT were applied on a twig and on the main stem of a 2-years
284 old pear sapling respectively (the sapling was kept in the laboratory at constant
285 temperature). The plant was watered before the beginning of the test and irrigation was
286 stopped during the 12-day long test. The environmental conditions were kept almost

287 constant, with a temperature of $20^{\circ}\text{C}\pm 1^{\circ}\text{C}$ and a relative humidity of $40\%\pm 5\%$. The
288 normal day/night cycles were mimicked by a 300 W growth lamp, providing solar
289 radiation from 6 am to 8 pm. The stemflow meter was calibrated by correlating the steady-
290 state signal recorded on selected days during day and night with the transpiration rate
291 measured by a balance.

292 Although the accuracy of stemflow meter to capture daily fluctuations of xylem water
293 flow rates could not be verified, it was deemed worth benchmarking the calibrated
294 stemflow meter against the measurement of a HCT as shown in Figure 10 (details of the
295 HCT measurement on the Pear sapling are reported in Dainese & Tarantino 2020). The
296 measurement of the transpiration rate by the stemflow was often interrupted due to
297 instability of the data acquisition system.

298 It can be observed that the sap flow meter captures the same day/night cycles as the
299 HCT. Overnight, transpiration rate attains a minimum and this corresponds consistently
300 to the highest xylem water pressure (lower xylem water tension). The transpiration rate
301 measured by the sapflow meter shows sharp increase at 6 am, when the lamp was switched
302 on and this is associated with the abrupt decrease in xylem water pressure. During the day,
303 the relationship between xylem water pressure and transpiration rate is clearly reversed.
304 Even if the stemflow meter is difficult to calibrate in the field (because transpiration rate
305 is more difficult to measure), the signal of a stemflow meter can be used to assess the
306 quality of HCT and psychrometer measurements.

307



308

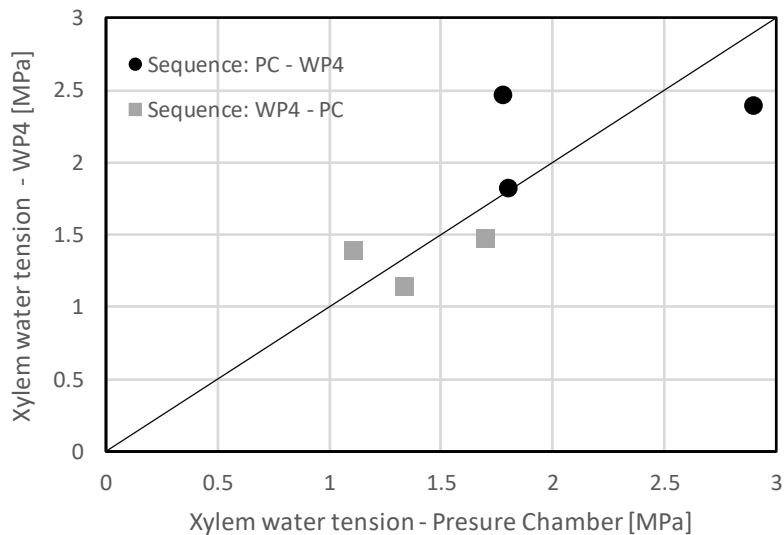
309 **Figure 10.** Comparison of the daily fluctuation of xylem water pressure measured by the HCT on
 310 a Pear sapling against the evapotranspiration rate measure by a stemflow meter.

311 2.5.2 Pressure chamber versus Chilled Mirror Psychrometer (WP4)

312 A comparison was made between the measurement by the pressure chamber and the
 313 WP4C Chilled-Mirror Psychrometer (Bulut & Leong 2008) by testing leaves taken from
 314 a tree on Strathclyde University campus. While on the tree, leaves were first cleaned with
 315 a tissue, wetted with a drop of distilled, gently scratched three times with sandpaper,
 316 wrapped with aluminium foil and let to rest for 10 minutes. Afterwards, leaves were
 317 excised, inserted in a plastic bag in the presence of a wet tissue to minimise evaporation
 318 (contact between the tissue and the leaves was avoided), and transported to the laboratory.
 319 In the laboratory, two sets of measurements were carried out. In the first series, suction
 320 was first measured in the WP4C and then in the Scholander Pressure Chamber. This

321 procedure was reverse in the second series where suction was first measured in the
322 Scholander Pressure Chamber and then in the WP4C.

323 The results of this exercise are shown in Figure 11. Although a very limited number of
324 measurements are compared, there seems to be a fair agreement between the two
325 techniques and the sequence adopted does not seem to affect significantly the
326 measurements and their alignment to a 1:1 line. This seems to suggest that evaporation
327 that may occur in either the Pressure Chamber or WP4C does not affect significantly the
328 measurement.



329

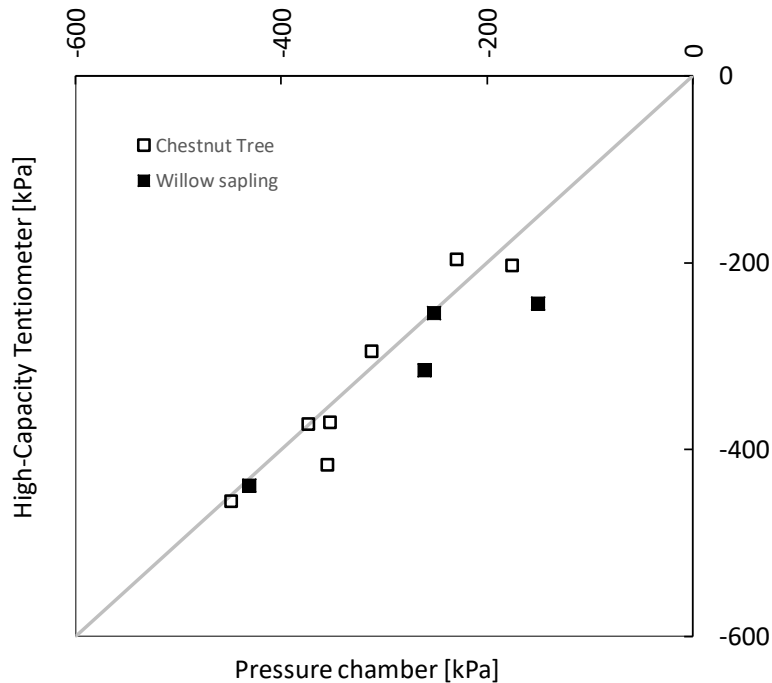
330 **Figure 11.** Comparison of Pressure Chamber versus Chilled Mirror Psychrometer (WP4)

331 measurements

332 2.5.3 *High-Capacity Tensiometer versus Pressure Chamber and Thermocouple*
333 *Psychrometer*

334 The three techniques that can be used to measure the xylem water tension, i.e. the High-
335 Capacity Tensiometer, the Thermocouple Psychrometer, and the Pressure Chamber were
336 benchmarked in two separate studies (Dainese & Tarantino, 2020; Dainese et al. 2020)
337 whose results are briefly summarised here.

338 High-capacity tensiometer was compared to the pressure chamber via measurements
339 of xylem water pressure on a Chestnut tree (in the field) and a Willow sapling (in the
340 laboratory) (Dainese & Tarantino, 2020). Pressure chamber measurements on Chestnut
341 leaves were taken on sets of six leaves, sampled from the same branch where the HCTs
342 were installed. The leaf wrapping time was set to 10 min. Pressure chamber measurements
343 on the Willow sapling were based on sets of three leaves with a wrapping time of at least
344 2h (higher wrapping time was required as the plant was under water stress conditions).
345 The comparison between the two measurement techniques is shown in Figure 12 and the
346 fair alignment to the line 1:1 can be taken as a cross validation of the two techniques.



347

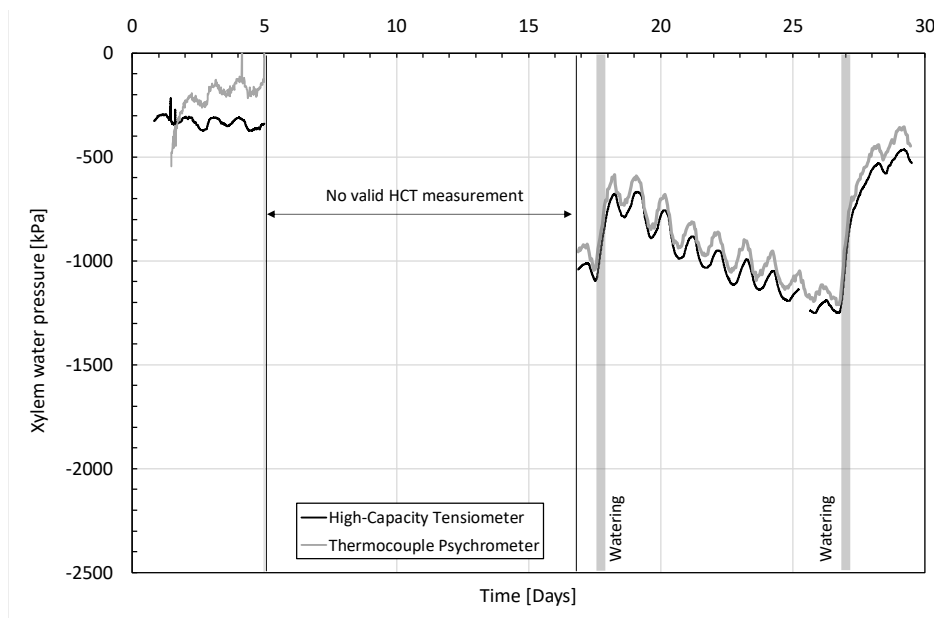
348 **Figure 12.** Comparison of Pressure Chamber versus High-Capacity Tensiometer measurements

349 (after Dainese & Tarantino 2020)

350 High-capacity tensiometer was compared to the thermocouple psychrometer via
 351 measurements of xylem water pressure on a Pear sapling (Dainese et al., 2020). Two high-
 352 capacity tensiometers and one thermocouple psychrometer were installed with a spacing
 353 of approximately 10 cm on the sapling stem with the thermocouple psychrometer between
 354 the two HCTs. The measurements by the two high-capacity tensiometers shown Figure 2
 355 are replotted in Figure 13 in terms of average and only for the time intervals where the
 356 measurement was considered valid. The same figure shows the measurement by the
 357 thermocouple psychrometer. It can be observed that xylem water pressure measurements
 358 are fairly consistent below -500 kPa and, again, this can be taken as a cross validation of

359 the two techniques. As discussed by Dainese et al. (2020), the thermocouple psychrometer
360 appears to be not accurate at xylem water pressures higher than -500 kPa. In this range,
361 the relative humidity is very close to saturation (> 99.5%) and becomes difficult to
362 measure accurately.

363 Figure 13 also shows that daily fluctuations recorded by the thermocouple
364 psychrometer and the high-capacity tensiometers are in phase. This demonstrates an
365 prompt response time of the two instruments considering they operate on the basis of very
366 different working principles (equilibrium via liquid and vapour phase for the high-
367 capacity tensiometers and the thermocouple psychrometer respectively).



368

369 **Figure 13.** Comparison of Thermocouple Psychrometer versus High-Capacity Tensiometer
370 installed on Cheery sapling (after Dainese et al., 2020)

371 **3 Measurements in soil**

372 Water flow in the vadose zone towards the plant is controlled by the soil unsaturated
373 hydraulic conductivity (which depends on volumetric water content), and the water
374 retention behaviour, i.e. the relationship between pore-water pressure and volumetric
375 water content. As a result, both pore-water pressure and water content need to be
376 monitored to characterise the water flow in the soil-plant continuum.

377 **3.1 Pore-water pressure**

378 Pore-water tension in the field was measured using the High-Capacity Tensiometer.
379 Boreholes having a diameter slightly larger than the tensiometer (~20mm) were drilled in
380 the proximity of the multi-point water content probes (described in the next section) with
381 the aid of a manual auger. The tensiometer was mounted at the end of a rod and pushed
382 down to the bottom of the borehole. A saturated paste made by mixing the finer fraction
383 of the soil extracted from the borehole and kaolin was interposed between the tip of the
384 tensiometer and the bottom of the borehole to ensure the hydraulic continuity. Evaporation
385 from the point of measurement was prevented by the very close gap between the rod and
386 the borehole wall. The tensiometer was left overnight to equilibrate and the measurement
387 was taken 18-24 h after the installation.

388 **3.2 Moisture content profile**

389 *3.2.1 Drill & Drop probe*

390 A convenient approach to measure water content is represented by water content profile
391 probes because a single installation can be used to capture the water content profile along
392 a vertical. Earlier concepts (Tarantino et al., 2008) required drilling a borehole, installing
393 a casing, and inserting the probe carrying multiple unprotected capacitive sensors into the
394 casing. However, pouring the grout in the annular gap between the borehole and the casing
395 often leaves air gaps that generate spurious measurements (Caruso et al. 2013). A new
396 water content profile probe has been recently commercialised where the capacitive sensors
397 are encapsulated into a single shaft. The performance of this probe is discussed and
398 validated in this section. The ‘Drill & Drop’ probe is manufactured by Sentek Sensor
399 Technologies, Australia, it can be up to 1.2 m long, and can include up to 12 capacitive
400 sensors spaced 100 mm.

401 The working principle of the probe is based on the correlation between the bulk dielectric
402 permittivity of the soil and its volumetric water content. The dielectric permittivity is in
403 fact strongly influenced by the presence of water within the grains, given that the relative
404 dielectric permittivity of pure water at 20°C is around 80, ranges between 10 and 30 for
405 roots (Mihai et al. 2019), it is between 3 and 5 for the solid phase in most soils (Tarantino
406 et al. 2008), and it is 1 for air. The dielectric permittivity is measured by the ‘Drill and
407 Drop’ capacitive sensors through the assessment of the soil capacitance (two rings on the
408 probe form the conductors of a capacitor filled by a composite dielectric medium that
409 includes the soil (Dean et al., 1987).

410 The probe requires the drilling of a 25mm diameter borehole within the soil, in which
411 the probe is inserted by simple pushing. The installation procedure does not rely on the
412 use of a grout. Contact is ensured by the tapered shape of the probe, which is 25 mm
413 diameter at its bottom and 30 mm diameter at its top. This minimises the presence of air
414 gaps between the probe and the soil (compared to the grout installation of the probes of
415 first generation). The installation procedure is demonstrated by the manufacturer through
416 a series of videos (Sentek Technologies, 2019).

417 *3.2.2 Effect of roots on the measurement of dielectric permittivity*

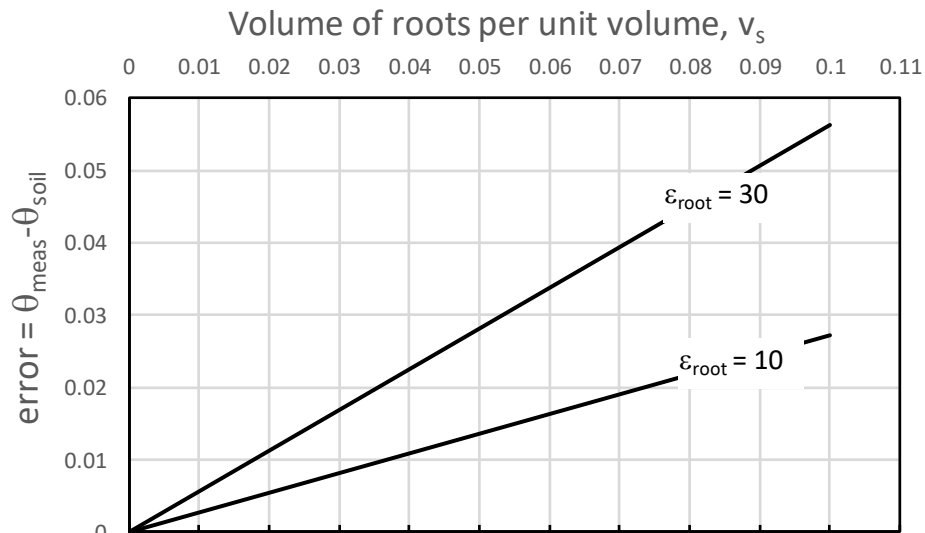
418 Soil volumetric water content θ is inferred from the measurement of the bulk soil dielectric
419 permittivity K_a . Empirical equations are generally used to correlate K_a to θ , e.g. Topp et
420 al. (1980) and Ledieu et al. (1986). These equations have been developed for the case of
421 mixtures made of solids, air, and (free) water and may no longer be applicable if a fourth
422 phase (i.e. roots) is present.

423 The error in the volumetric water content measurement introduced by the presence of roots
424 was estimated by considering the theoretical relationship (Complex Refractive Index
425 Model, CRIM) between the soil volumetric water content θ and the bulk soil dielectric
426 permittivity K_a . This theoretical model was first validated against traditional empirical
427 equations by considering a three-phase mixture and then used to estimate the error
428 associated with the presence of roots by considering a four-phase mixture. The following
429 Equation was derived for the error in the measurement of the soil volumetric water content
430 θ (see Eq. [12] in the Appendix 1)

$$\Delta\theta_{error} = \frac{\sqrt{\varepsilon_a} - \sqrt{\varepsilon_r}}{\sqrt{\varepsilon_w} - \sqrt{\varepsilon_a}} v_r \quad [1]$$

431 where v_r is the volume fraction of roots and ε_a , ε_w , and ε_r are the values of dielectric
 432 permittivity of the air, water, and roots respectively. This error is plotted in Figure 14 for
 433 the values of root dielectric permittivity that bound the range observed experimentally
 434 ($\varepsilon_r=10-30$).

435 The error clearly depends on the volume fraction of roots v_r and can be significant for high
 436 values of v_r . For the measurements presented in this paper, the volume fraction of roots in
 437 the range of depths 0-1.2 m has an average value of 0.005 with a standard deviation of
 438 0.005 (Appendix 2). In this set of measurements, the error introduced by the presence of
 439 roots was therefore negligible.



440
 441 *Figure 14: Error in water content measurement associated with the presence of roots*

442 3.2.3 *Effect of air gap on water content measurement*

443 The presence of air gaps at the interface between the probe and the soil, which are
444 minimised but not eliminated with the encapsulated probe, can severely affect the
445 measurement, given the ratio between the dielectric permittivity of air and water is 1:80.
446 It is therefore important to identify approaches to validate the measurement of water
447 content.

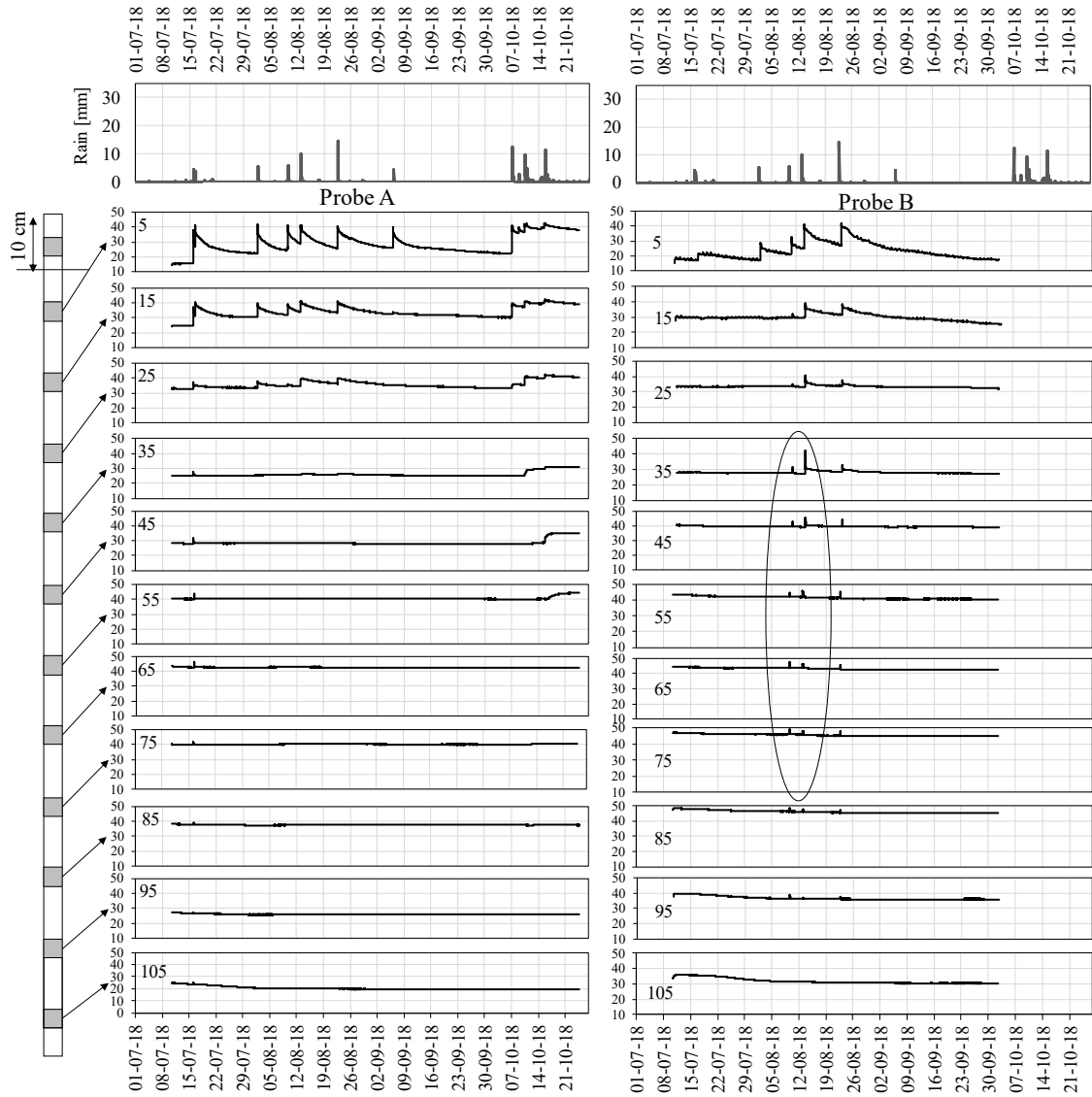
448 A clear example of measurements affected or not by the presence of an air gap is shown
449 in Figure 15, which shows the measurement by two profile probes installed in
450 Restinclières (France) in silty soil (20% clay, 56% silt, 22% sand), among poplar trees
451 (Probe A) and in an adjacent open field (Probe B). The probes were installed in early July
452 and the graph represents approximately 4.5 months of measurements.

453 The capacitive sensors are represented individually, ordered by the vertical position on
454 the single probe. The number in each box represents the depth of the single sensor from
455 the soil ground level in centimetres. There is a peak in water content of the probes in
456 correspondence of rain events. For the case of probe A, the peaks disappear at a depth
457 starting from 35cm (with the exception of the first rain event) whereas peaks persist down
458 to a depth of 75 cm for probe B (encircled). While the peak in the shallow layer disappears
459 slowly, as water drains or evaporates, spikes in the lower levels (35-75) indicate a spurious
460 effect associated with the air gap filling with water during the rain event and quickly
461 emptying afterwards.

462 The effect of the an air gap on the water content measurement is represented
463 schematically in Figure 16**Error! Reference source not found..a**. In stage 1 and 3 the

464 air-filled gap leads to an underestimation of the water content measurement, while the
465 water accumulated during the rain event leads to an overestimation of the water content
466 of the soil surrounding the probe.

467 The major problem to be addressed in the water content measurement is to quantify the
468 underestimation of measurement in stages 1 and 3 once the presence of an air gap is
469 recognised by the peak occurring in stage 2.

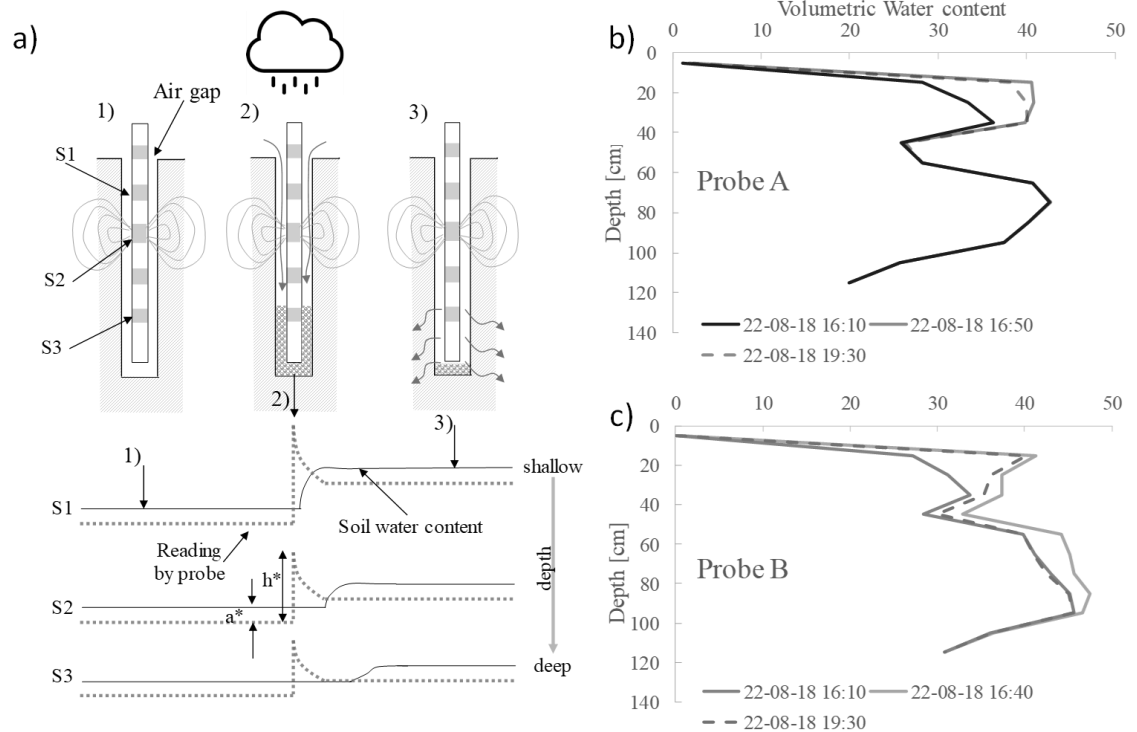


471

472 *Figure 15: Representation of Volumetric Water Content evolution over time at different depths for*
473 *2 different 'Drill and Drop' probes.*

474

475



476

477 *Figure 16: (a) Effect of air gap on measurement (a.1) before, (a.2) just after, and (a.3) long after a*
 478 *rain event. Water content profile in correspondence of stage a.1, a.2 and a.3 during the rain event*
 479 *of the 22/08/18 for (b) probe A and (c) probe B*

480 *3.2.4 Assessing experimentally the error associated with the presence of air gap (from*
 481 *water balance)*

482 The experimental data were analysed with reference to the rain event occurring on the
 483 22/08/2018 for probe A (Figure 16.b) and probe B (Figure 16.c) respectively. The rain
 484 event was registered by a CIRAD weather station placed at approximately 1 km distance
 485 was characterised by an amount of 14.7 mm (volume per unit area) and occurred between
 486 16:00 and 17:00 (the time resolution of the weather station is 60 min).

487 The three water content profiles correspond to the condition before the rain (time
488 16:10), after the rain event showing the maximum water content variation (times 16:40 or
489 17:10), and ~3h after the rain event (time 19:30). The amount of infiltrated rainwater can
490 be in principle derived from the integration of the change of water content profile
491 measured before and after the rainfall. The rainfall amount estimated by the probe is
492 compared with the actual rainfall amount in Table 1.

493 For the case of probe A, the measurement of infiltrated rainwater after approximately
494 3 hours (stage 3 minus stage 1) is comparable with the measurement at the peak (stage 2
495 minus stage 1) indicating a negligible air gap. This is confirmed by the close match
496 between the actual rainfall amount and the one inferred from the profile probe.

497 For the case of Probe B, the amount of rainfall derived from the water content profile
498 at peak (36.2 mm, stage 2) is significantly higher than the one derived after ~3h (13.9 mm,
499 stage 3). This indicates again that the water content profile measured by Probe B at peak
500 (stage 2) is biased by the presence of water accumulating in the gap between the probe
501 and the surrounding soil (water content accumulated in the ground at peak and after ~3h
502 should not be significantly different). The water accumulation inferred from these
503 measurements is consistent with the anomalous peaks recorded by the relatively deep
504 sensors as shown in Figure 15.

505 Although it appears evident that the measurement at peak should be discarded, the
506 problem to be addressed is whether the presence of an air gap is affecting significantly the
507 measurements in stages 1 and 3. This question can be easily answered by comparing the
508 infiltrated rainwater derived from Probe B after ~3 h with the actual rainfall amount, 13.9

509 mm versus 14.7 mm respectively. The straightforward conclusion is that the presence of
 510 the air gap does not affect significantly the measurement of the water content profile once
 511 water is no longer filling the gap.

512

513 *Table 1: Rain event on 22/08/2018. Comparison of volume of rainwater per unit area calculated*
 514 *from 'Drill & Drop' measurements with rainfall amount.*

	Based on Raw data		Corrected for air gap	
	At peak [mm]	After ~3 h [mm]	At peak [mm]	After ~3 h [mm]
Probe A	17.4	15.6	15.6	15.7
Probe B	19.2	13.9	13.5	14.2
Rainfall amount (by weather station)			14.7 mm	

515 *3.2.5 Estimating the error associated with the presence of air gap from using dielectric*
 516 *permittivity mixing model*

517 An approach to assess the effect of the air gap on the water content measurement is
 518 presented here that does not require the comparison with the actual rainfall amount, which
 519 may not be always available. The volumetric water content returned by the probe, θ_{measured} ,
 520 is based on the measured apparent dielectric permittivity K_{measured} . According to (Ledieu
 521 et al. 1986), the following correlation can be established:

$$\theta_{measured} = a \cdot \sqrt{K_{measured}} - b \quad [2]$$

522 where a and b are empirical coefficients ($a=0.1138$ and $b=0.1758$). The dielectric
 523 permittivity read by the probe is generated by the dielectric permittivity values of the soil
 524 and the gap (filled with either water or air) weighted by their volume fractions. As a first
 525 approximation, the following mixing model can be considered:

$$\sqrt{K_{measured}} = \frac{x_{gap}}{L} \sqrt{K_{gap}} + \frac{L - x_{gap}}{L} \sqrt{K_{soil}} \quad [3]$$

526 where x_{gap} is the gap between the probe and the surrounding, L is the radius of the
 527 cylindrical sampling volume around the probe ($L=10$ mm), K_{soil} and K_{gap} are the dielectric
 528 permittivity values of the soil and the gap respectively. For each of the three stages
 529 considered, the soil dielectric permittivity can be written as:

$$K_{soil,i} = \left(\frac{\theta_{measured,i} + b}{a} - \frac{x_{gap}}{L} \sqrt{K_{gap,i}} \right) \cdot \frac{L}{L - x_{gap}} \quad [4]$$

530 with $i=1$ to 3 and $K_{gap,1} = K_{gap,3} = K_{air}$, and $K_{gap,2} = K_{water}$. In turn, the volumetric water
 531 content of the soil θ_{soil} can be associated with the soil dielectric permittivity:

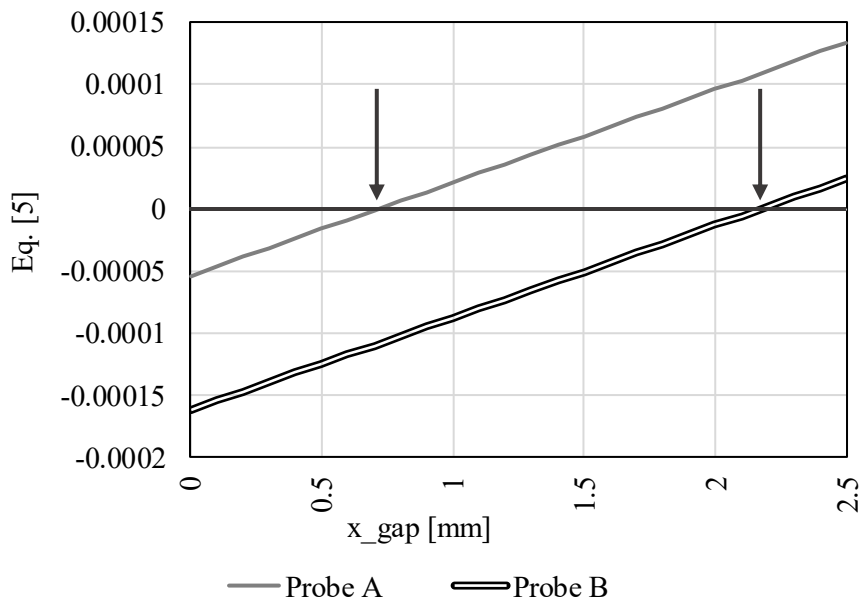
$$\theta_{soil} = a \cdot \sqrt{K_{soil}} - b \quad [5]$$

532 Let us assume that the water accumulating in the gap in stage 2 infiltrates radially into
 533 the sampling volume of radius L . The volume balance equation can therefore be written
 534 as follows:

$$\pi \left[L^2 - (r_p + x_{gap})^2 \right] \left(\int \theta_{soil,3} dz - \int \theta_{soil,2} dz \right) - h_{probe} \quad [6]$$

$$\cdot \pi \left[(r_p + x_{gap})^2 - r_p^2 \right] = 0$$

535 where r_p is the radius of the probe. The four Equations [4] and [6] can be used to derive
 536 the four unknowns $K_{soil,i}$ and x_{gap} . The left-hand side of Equation [6] is plotted versus x_{gap}
 537 in Figure 17. The gap resulting from this calculation is 0.7 mm for Probe A and 2.2 mm
 538 for Probe B. This gap can be then used to correct the values of water content measured by
 539 the probe via Equations [4] and [5]. As shown in Table 1, the values of rainfall amount
 540 derived in stages 2 and 3 are now comparable and very close to the actual rainfall amount.



541

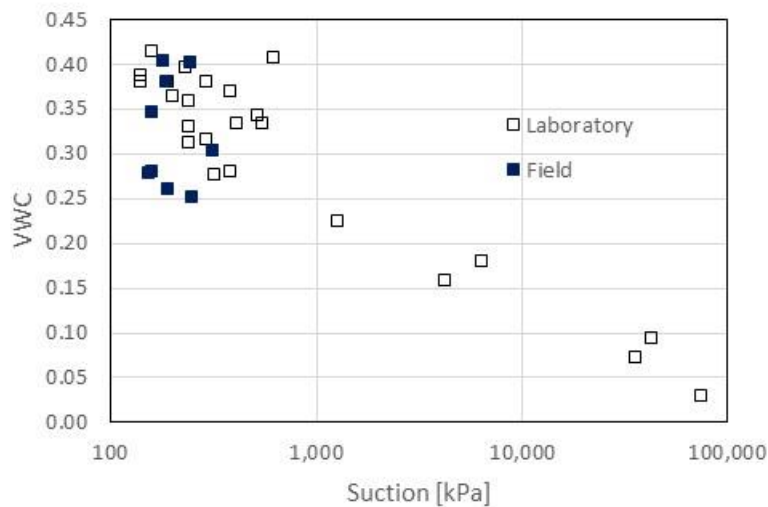
542 *Figure 17: Estimation of the air gap*

543

544 **3.3 Field versus laboratory water retention data**

545 Figure 18 shows the water retention data of Restinclières soil measured in the laboratory
546 on samples taken from the field via boreholes drilled close to the probes and in the field.
547 Suction measurement in the laboratory was conducted using a chilled mirror psychrometer
548 (WP4C). The void ratio and the gravimetric water content (used to derive the volumetric
549 water content) were derived by pushing a cutting ring into the sample, trimming the excess
550 material, determining the total volume from the inner size of the cutting ring, and oven-
551 drying the sample. Some of the samples were was dried and some wetted to explore a
552 wider range of suction. Suction in the soil at various depths was measured via the High-
553 Capacity Tensiometers, as previously described, while the volumetric water content was
554 assessed via the Probe A placed in proximity of the suction sensors. Volumetric water
555 content data were paired with suction measurement data taken at similar depth.

556 Figure 18 shows a fair agreement between laboratory and field data. Water retention data
557 are quite scattered due to the intrinsic heterogeneity of a natural deposit conditions.



558

559 *Figure 18: Comparison of water retention data measured in the laboratory and in the field*

560 **4 Electrical Resistivity Tomography to guide installation of local** 561 **sensors**

562 **4.1 Concept idea**

563 Local sensors such as such as the ‘Drill and Drop’ and the HCT and other local sensors
564 for measurement of suction and water content (Tarantino et al. 2008) offer the possibility
565 of investigating the variation of moisture content and suction in the field. However, there
566 are two major challenges concerning the design of monitoring systems based on local
567 sensors: (i) where to install the sensors to ensure that the local measurement is
568 representative of the area to investigate and (ii) how to extrapolate the spatial distribution
569 of measured localised variables. These issues can be addressed successfully by integrating
570 the geotechnical monitoring with electrical geophysical survey (Electrical Resistivity
571 Tomography - ERT). Electrical resistivity is a function of multiple parameters including
572 water content, mineralogy, pore structure, chemical composition of pore fluid, and
573 temperature (Samouëlian et al., 2005). However, the tendency of decreasing resistivity
574 with increasing water saturation makes this method appealing for measuring a variety of
575 different hydrologic processes. Conventional ERT surveys have been used in many
576 applications to monitor changes in moisture content patterns, including around trees (Fan
577 et al., 2015; Cassiani et al., 2015, 2016; Consoli et al., 2017; Mary et al., 2018). Thus,

578 preliminary ERT surveys can be of great help to characterise an area or a geo-structure
579 and optimise location of moisture sensors.

580 **4.2 Investigating resolution by inverting synthetic model**

581 The imaging of electrical resistivity in the subsurface by ERT is based on the inversion of
582 a set of resistance measurements on a given array of electrodes. Given the nonlinearity of
583 the underlying forward problem, electrical inversion schemes proceed in iterations
584 through modelling runs looping forward, comparing predicted and measured data, and
585 updating the estimate of the electrical resistivity distribution with a view to reducing data
586 misfit. In this work, all forward and inversion modelling was performed using ResIPy
587 v2.2.2 (Blanchy *et al.*, 2020).

588 To examine whether the ERT could help address these two key challenges, synthetic
589 models for the forward modelling exercise were created based on the observations made
590 by Dainese (2020) at an experimental agroforestry plot used for agricultural studies in
591 Restinclières, France. The author monitored the distribution of moisture content over wet
592 and dry periods by installing ‘Drill and Drop’ sensors in different locations in the forestry
593 plot and in the open field. Three different water regimes were observed close to the trees,
594 in the depth ranges of 0-50cm, 50-100 cm, and >100cm. In the first 50cm depth, moisture
595 increased (from 0.2 to 0.35 volumetric moisture content) in the wet period, and decreased
596 (from 0.35 to 0.25) in the dry period. Between 50 and 100cm there was no changes in
597 moisture content. In the wet period, below 100cm, a decrease of moisture (from 0.25 to
598 0.2) was observed extending below the 120cm depth of the ‘Drill and Drop’ and that could

599 not be obviously detected by the sensor. Additionally, the author also noticed changes in
600 moisture on the first half meter depth, laterally away from the tree (increasing in the wet
601 period and decreasing in the dry) and below 1m depth (decreasing in both wet and dry
602 periods).

603 It was realised ‘a posteriori’ that the probe should have been installed deeper and the
604 question was asked about whether a preliminary ERT investigation would have helped
605 identifying in advance the zones where moisture content changed significantly. In other
606 words, whether the ERT could resolve the soil moisture regime down to 1m, which is the
607 length of the Drill and Drop’ sensor.

608 The approach pursued in this paper was to generate synthetic ERT data representative
609 of the observations made by Dainese (2020) and compare the inverted ERT model with
610 the original synthetic one. Synthetic models are those in which resistivity values are
611 assigned to elements of the mesh created according to the problem it is representing. This
612 model is then forward modelled (via ResIPy), i.e. the apparent resistivity pseudosection is
613 calculated for the defined 2D subsurface model. Finally, the data generated by the forward
614 model are inverted producing the inverted model, which can then be compared with the
615 original synthetic model created.

616 The resistivity values chosen to represent the water content differences observed by
617 Dainese (2020) were based on a Time Domain Reflectometry (TDR) survey carried out at
618 Rest and Be Thankful site in Scotland (Gladin, 2018). In this survey, TDR probes were
619 installed on the scar of a vegetated hillslope. TDR data was acquired after probes
620 installation and after an artificial rainfall simulated by pouring water from the top of the

621 slope. Results demonstrated that for the clayey silt material at the site, a volumetric water
622 content of 0.2, 0.3 and 0.4 correspond to a resistivity of 400, 215 and 150 Ω m respectively.
623 If the middle resistivity value (215 Ω m) is established as the reference, then the remaining
624 values are representative of 0.1 increase and decrease of moisture content.

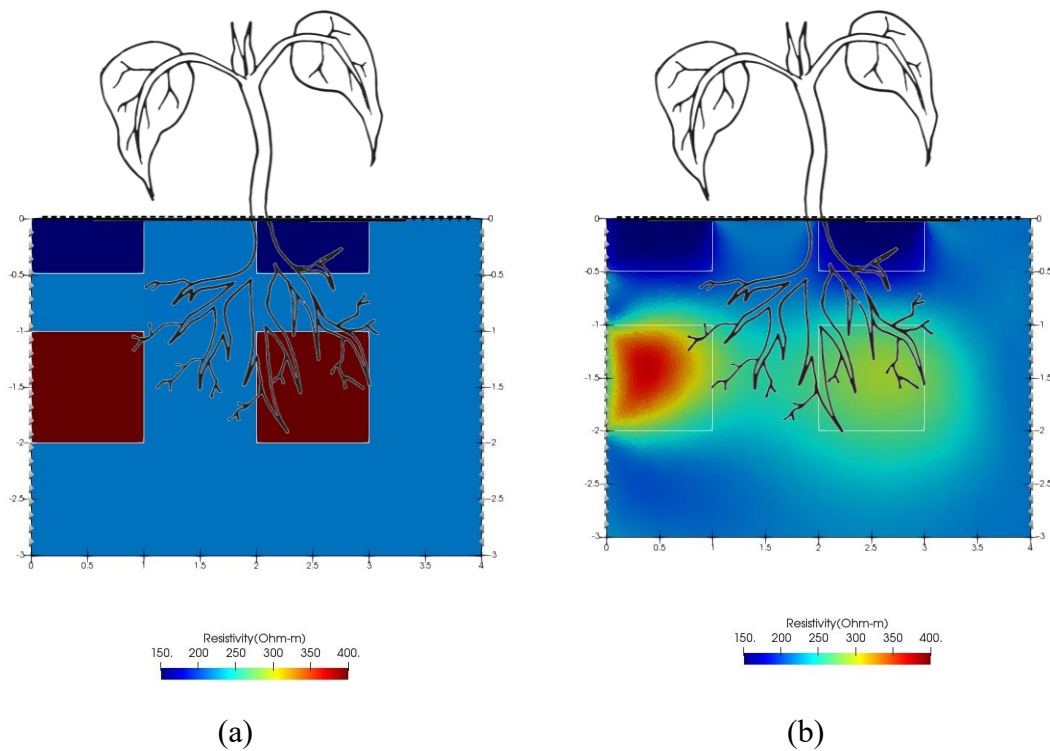
625 Thus, these synthetic models (Figure 19.a-c) have a background of 215 Ω m and a few
626 regions of lower or higher resistivity depending on the period it represents. Figure 19.a is
627 representative of the wet period reported by Dainese (2020) with two lower resistivity
628 (150 Ω m) 0.5m² regions closer to the surface below the tree ([2.0,0.0]; [3.0,-0.5]) and away
629 from the tree ([0.0,0.0]; [1.0,-0.5]) and with two higher resistivity (400 Ω m) 1m² regions
630 below the tree ([2.0,-1.0]; [3.0,-2.0]) and away from the tree ([0.0,-1.0]; [1.0,-2.0]). Figure
631 19.c represents the dry period reported by Dainese (2020), with two 0.5m² regions of high
632 resistivity (400 Ω m) closer to the surface and one 1m² region also with high resistivity
633 away from the tree starting at 1m depth.

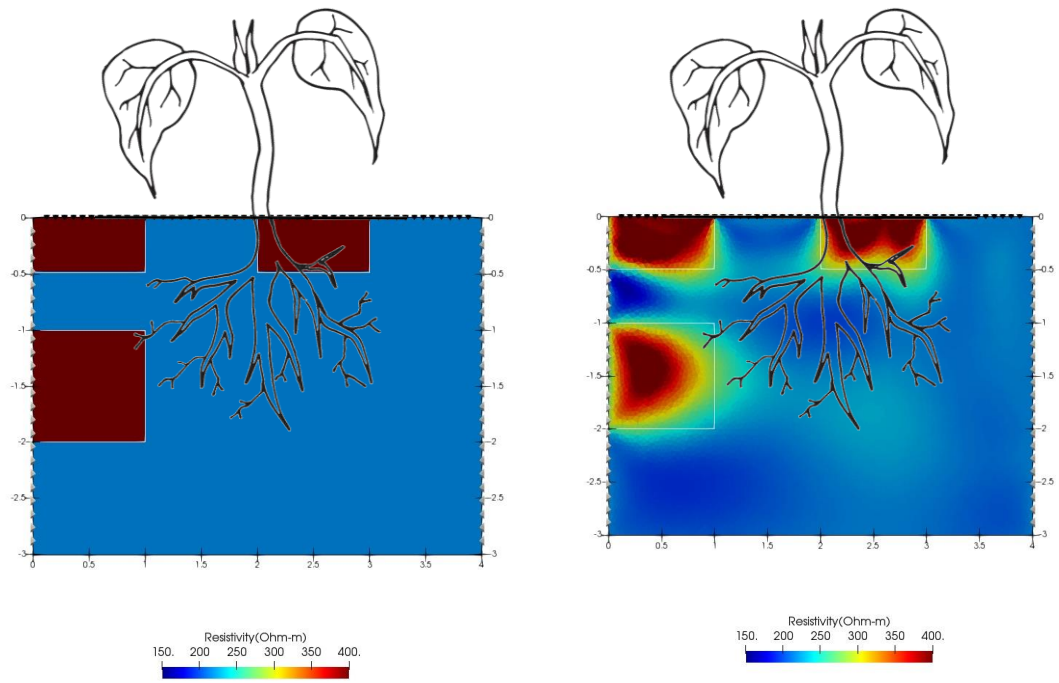
634 The measurement scheme designed was a mixture of in-hole (dipole-dipole and
635 Schlumberger, skip 0 to 6) and cross-borehole (AM-BN, AB-MN, A-BMN and A-MBN,
636 skip 0 to 6), totalling 10,298 independent data points (Sensitivity - Figure 20).

637 The inverted results (Figure 19.b-d) show that the superficial region of low (wet
638 period) and high (dry period) resistivity is well captured both in terms of geometry and
639 resistivity value, regardless of whether the resistivity value is higher or lower than the
640 background resistivity. The 1m² region of low resistivity in the wet period, and high
641 resistivity in the dry period that starts at 1m depth and is located away from the tree is also

642 well captured in terms of geometry and resistivity value. Finally, the 1m² resistivity area
643 below the tree (starting at 1m depth), that is present in the model representative of the wet
644 period (Figure 19.b), can still be easily identified, despite the fact that this is a region of
645 low sensitivity (Figure 20).

646 Therefore, this suggests that ERT could guide the installation of these local sensors.
647 If ERT surveys had been performed by Dainese (2020) prior to the installation of the ‘Drill
648 and Drop’ sensors, the author could have potentially recognised that changes in moisture
649 content were prominent at depths below 1m; in this way the author could have drilled a
650 few deeper boreholes to capture moisture changes at deeper locations.

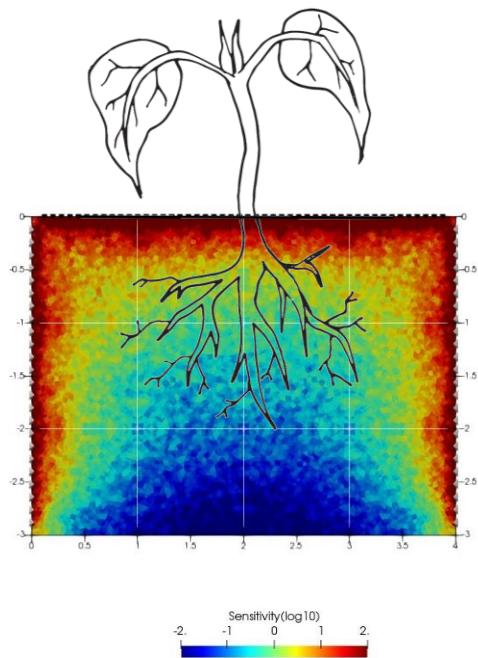




(c)

(d)

651 *Figure 19 Model representative of the wet period: (a) Synthetic model, (b) Inverted model; Model*
 652 *representative of the dry period: (c) Synthetic model, (d) Inverted model*



653

654 *Figure 20. Measurement scheme sensitivity*

655 **5 Conclusions**

656 The paper has presented a monitoring concept for the soil-plant continuum and focused
 657 on the measurement of water potential and flow rate of xylem water and the monitoring
 658 of soil suction and water in proximity of a tree.

659 Three different techniques for the measurement of xylem water tension, i.e. High-
 660 Capacity Tensiometer (HCT), Thermocouple Psychrometer (TP), and Pressure Chamber
 661 (PC), have been presented. Critical aspects of the experimental procedure including
 662 calibration, data quality check, and measurement precision have been investigated and
 663 measurement accuracy has been probed by cross-validation.

664 The HCT is the same prototype used for more than two decades in the geotechnical
665 engineering field. Details of the installation on the stem have been presented and discussed
666 to enable other researchers installing their own tensiometer. It has been shown that the
667 HCT has to be installed in pairs. In general, the measurement shows excellent precision
668 and differences between HCTs installed at close distance on the stem (<100-200 mm) are
669 generally less than 50 kPa. However, significant deviations may occur and this invalidates
670 the measurement. Deviations may occur due to ongoing cavitation or healing at the
671 measuring site.

672 The thermocouple psychrometer requires calibration by exposure of the sensor to NaCl
673 solutions of known concentration (osmotic suction). The calibration method based on the
674 use of a filter paper as proposed by the manufacturer can be potentially biased by the
675 matric suction generated by the filter paper if menisci form at the filter paper-air interface.
676 For this reason, calibration was carried out by exposing the sensor to free NaCl solutions
677 considering different air gaps between the solution and the sensor. It was finally
678 demonstrated that the procedure based on the filter paper provides reliable results. It was
679 also shown that the signal recorded by the sensor depends on both the Cooling Time (the
680 time whereby the current is circulated in the thermocouple) and the Wait Time (the time
681 at which the signal is recorded) and the same setting should be therefore used for
682 calibration and measurement.

683 As for the measurement by the Pressure Chamber, the leaf needs to be wrapped with
684 aluminium foil to establish 'hydrostatic conditions before excision according to the
685 manufacturer. It has been shown that the leaf should remain wrapped even when placing

686 it in the Pressure Chamber. The Pressure Chamber measurement appears to show
687 precision better than 100 kPa.

688 It was finally shown the measurements by these three techniques are highly
689 consistent, with the exception of the Thermocouple Psychrometer at xylem water tensions
690 below ~500 kPa.

691 The paper has therefore focused on the monitoring of soil suction using the High-
692 Capacity Tensiometer and the water content using a profile probe of second generation,
693 which is fully encapsulated and does not require the pre-installation of a casing. It was
694 shown that the major problem in water content measurement is the formation of a gap
695 between the probe and the surrounding soil. An approach has been presented to i) identify
696 the presence of the gap and ii) quantify the error associated with such a gap and correct
697 the measurement. The combined measurements of soil suction and water content in the
698 field was successfully benchmarked against water retention data acquired in the laboratory
699 in samples taken from the field.

700 Finally, it has been shown that Electrical Resistivity Tomography (ERT) can be very
701 useful to complement the local measurements of water content by the profile probe by
702 allowing capturing the spatial variability of the soil moisture distributions in vegetated
703 areas to guide the installation of these local sensors if ERT survey are carried out
704 preliminarily.

705 **Acknowledgement**

706 The authors wish to acknowledge the support of the European Commission via the Marie
707 Skłodowska-Curie Innovative Training Networks (ITN-ETN) project TERRE 'Training
708 Engineers and Researchers to Rethink geotechnical Engineering for a low carbon future'
709 (H2020-MSCA-ITN-2015-675762)

710

711 APPENDIX 1 – EFFECT OF ROOTS ON SOIL WATER CONTENT

712 MEASUREMENT

713 Soil water content θ is inferred from the measurement of the bulk soil dielectric
714 permittivity K_a . Empirical equations are generally used to correlate K_a to θ , e.g. Topp et
715 al. (1980) and Ledieu et al. (1986). However, the relationship between K_a and θ can also
716 be derived theoretically using a dielectric permittivity mixing model and this allows for
717 the quantification of the effect of roots on the water content measurement.

718 The simplest dielectric permittivity mixing model is the Complex Refractive Index
719 Model (CRIM) (Leão et al. 2015). This model is first assessed for the case of a three-phase
720 mixture (unsaturated soil in the absence of roots) and then extended to the case of a four-
721 phase mixture (unsaturated soil with the presence of roots) to assess the error in soil water
722 content measurement associated with the presence of roots in the measurement sampling
723 volume.

724

725 *Three-phase mixture (unsaturated soil in the absence of roots)*

726 According to Birchak et al. (1974), the soil bulk dielectric permittivity for a three-phase
 727 mixture can be expressed as follows:

$$\sqrt{K_a} = v_a\sqrt{\varepsilon_a} + v_w\sqrt{\varepsilon_w} + v_s\sqrt{\varepsilon_s} \quad [7]$$

728 where v_a , v_w , and v_s are the volume fractions of the air, water, and solids respectively and
 729 ε_a , ε_w , and ε_s are the values of dielectric permittivity of the air, water, and solids
 730 respectively.

731 Since

$$v_w = \frac{V_w}{V} = \theta$$

$$v_s = \frac{V_s}{V} = \frac{V_s}{M_s} \frac{M_s}{V} = \frac{\rho_d}{\rho_s} \quad [8]$$

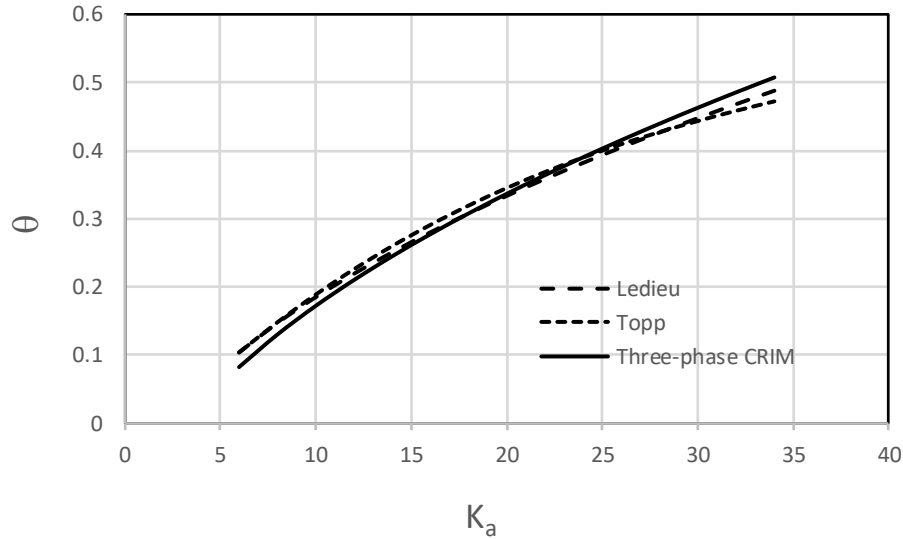
$$v_a = 1 - v_s - v_w = 1 - \frac{\rho_d}{\rho_s} - \theta$$

732 where V is the total volumes, V_w and V_s the volumes of water and solids respectively, M_s
 733 is the mass of solids, ρ_d and ρ_s the dry density and the density of the solids respectively.
 734 By combining Eqs. [7] and [8], a calibration curve can be derived, which has the same
 735 functional form of the equation proposed by Ledieu et al. (1986):

$$\theta = \left[\frac{1}{\sqrt{\varepsilon_w} - \sqrt{\varepsilon_a}} \right] \sqrt{K_a} - \left[\frac{\sqrt{\varepsilon_a} - (\sqrt{\varepsilon_a} - \sqrt{\varepsilon_s}) \frac{\rho_d}{\rho_s}}{\sqrt{\varepsilon_w} - \sqrt{\varepsilon_a}} \right] \quad [9]$$

736 This equation is compared with the very popular empirical equations presented by Topp
 737 et al. (1980) and Ledieu et al. (1986) respectively in Figure 21. It can be seen that Eq.

738 [9] is essentially equivalent to these two empirical equations and can therefore serve as a
 739 basis to assess the error associated with the presence of roots.



740

741 *Figure 21. Comparison of a three-phase CRIM with common empirical calibration equations*
 742 *($\epsilon_a=1$, $\epsilon_s=6$, $\epsilon_w=80$, $\rho_d=1.5$ g/cm³, $\rho_s=2.7$ g/cm³)*

743

744 *Four-phase mixture (unsaturated soil with the presence of roots)*

745 The mixing model for a four-phase mixture can be written as follows:

$$\sqrt{K_a} = v_a\sqrt{\epsilon_a} + v_w\sqrt{\epsilon_w} + v_s\sqrt{\epsilon_s} + v_r\sqrt{\epsilon_r} \quad [10]$$

746 By combining Eqs. [7] and [10], the following calibration curve is derived for the case
 747 where roots are present in the measurement sampling volume

748

$$\theta = \left[\frac{1}{\sqrt{\varepsilon_w} - \sqrt{\varepsilon_a}} \right] \sqrt{K_a} - \frac{\sqrt{\varepsilon_a} - (\sqrt{\varepsilon_a} - \sqrt{\varepsilon_s}) \frac{\rho_d}{\rho_s} - (\sqrt{\varepsilon_a} - \sqrt{\varepsilon_r}) v_r}{\sqrt{\varepsilon_w} - \sqrt{\varepsilon_a}} \quad [11]$$

749 where ε_r and v_r are the dielectric permittivity and volume fraction of roots respectively.

750 If the soil volumetric water content is still estimated using Eq. [7] even if roots are

751 present in the soil (as is the case of commercial probes where the output is returned

752 directly in terms of water content), the error can be quantified by considering the

753 difference between Eqs. [9] and [11] as follows:

$$\Delta\theta_{error} = \frac{\sqrt{\varepsilon_a} - \sqrt{\varepsilon_r}}{\sqrt{\varepsilon_w} - \sqrt{\varepsilon_a}} v_r \quad [12]$$

754

755 APPENDIX 2 – ROOT DENSITY AND ROOT VOLUME FRACTION AT

756 RESTINCLIERES SITE

757 The root volume fraction was determined on core samples extracted from boreholes drilled

758 at Restinclieres site. The total volume of the core sample was calculated from its length

759 and the inner diameter of the casing (85 mm). The length of the core sample contained in

760 the casing essentially coincided with the penetration in the ground indicating that

761 negligible compression occurred during penetration. The root volume was assessed

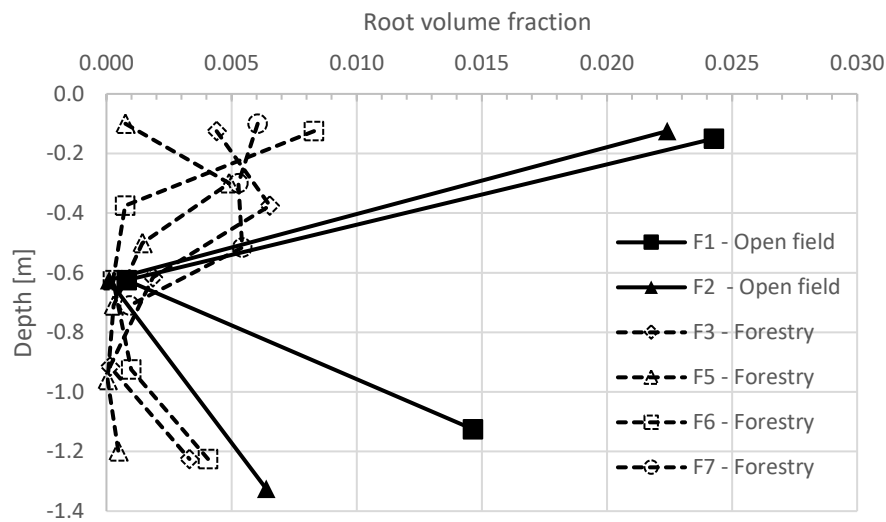
762 through the procedure described in detail by Dias (2019) briefly summarised here. Core

763 samples were washed through 2mm sieve in order to collect the roots. These were placed

764 on a scanner to acquire a high-resolution 2D image. Root dyeing was not required as root

765 natural colour allowed for sufficient contrast. The software WinRhizo (Arsenault et al.

766 1995) was used to analyse the images and to obtain the root cumulative volume. The roots
 767 were then removed from the scanner and placed in an oven at approximately 40°C for
 768 several days in order to obtain the dry weight and, hence, to calculate the root dry density.
 769 When the scan of all the roots contained in a core sample was considered to be excessively
 770 time consuming given the amount of roots contained, only part of the roots was scanned
 771 and the calculated volume was related to the total core sample volume proportionally to
 772 the root dry mass.



773
 774 *Figure 22. Profiles of root density at Restinclieres site*

775

776 **References**

777 Alcántara-Ayala, I., Esteban-Chávez, O. and Parrot, J-F. (2006). Landsliding related to
 778 land-cover change: A diachronic analysis of hillslope instability distribution in the

779 Sierra Norte, Puebla, Mexico. CATENA, 65: 152-165. DOI:
780 10.1016/j.catena.2005.11.006.

781 Arsenault J.-L., S. Pouleur, C. Messier & R. Guay. 1995. WinRHIZO, a root-measuring
782 system with a unique overlap correction method. HortScience, Vol. 30, pp. 906.
783 (Abstract).

784 Balling, A. & Zimmermann, U. (1990). Comparative measurements of xylem pressure of
785 Nicotiana plants by means of the pressure bomb and pressure probe. *Planta*, 182(3):
786 325-338

787 Birchak J R, Gardner C G, Hipp J E and Victor J M 1974 High dielectric constant
788 microwave probes for sensing soil moisture Proc. IEEE 62 93–8

789 Blanchy, G., Saneiyani S., Boyd, J., McLachlan, P., Binley, A. (2020) ResIPy, an intuitive
790 open source software for complex geoelectrical inversion/modeling. Computers and
791 Geoscience 137: 104423

792 Boyer, J. S., 1967. Leaf water potentials measured with a pressure chamber. *Plant*
793 *Physiology*, 42(1):133-7. DOI: 10.1104/pp.42.1.133.

794 Brown P., and Tanner, C. (1981). Alfalfa water potential measurement: a comparison of
795 the pressure chamber and leaf dew-point hygrometers. *Crop science*, 21(2), 240-244

796 Bulut, R. & Leong, E., (2008). Indirect measurement of suction. *Geotechnical and*
797 *Geological Engineering*, 26: 633-644. DOI: 10.1007/s10706-008-9197-0.

798 Canny, M. J. (1977). Flow and transport in plants. *Annual Review of Fluid Mechanics*, 9:
799 275–296.

800 Caruso, M, Avanzi, F. & Jommi, C. (2013). Influence of installation procedures on the
801 response of capacitance water content sensors. DOI: 10.1201/b13890-15.

802 Cassiani, G., Boaga, J., Rossi, M., Putti, M., Fadda, G., Majone, B., Bellin, A., 2016. Soil-
803 plant interaction monitoring: Small scale example of an apple orchard in Trentino,
804 North-Eastern Italy. *Science of the Total Environment*, 543, pp. 851-861.

805 Cassiani, G., Boaga, J., Vanella, D., Perri, M. T., Consoli, S., 2015. Monitoring and
806 modelling of soil-plant interactions: The joint use of ERT, sap flow and eddy
807 covariance data to characterize the volume of an orange tree root zone. *Hydrology
808 and Earth System Sciences*, 19 (5), pp. 2213-2225.

809 Consoli, S., Stagno, F., Vanella, D., Boaga, J., Cassiani, G., Roccuzzo, G., 2017. Partial
810 root-zone drying irrigation in orange orchards: Effects on water use and crop
811 production characteristics. *European Journal of Agronomy*, 82, pp. 190-202.

812 Corti, T., Wüest, M., Bresch, D. & Seneviratne, S. (2011). Drought-induced building
813 damages from simulations at regional scale. *Natural Hazards and Earth System
814 Sciences*, 11: 3335-3342. DOI: 10.5194/nhess-11-3335-2011.

815 Dainese R, Tedeschi G, Fourcaud T and Tarantino A (2020a). Measurement of xylem
816 water pressure using High-Capacity Tensiometer and benchmarking against Pressure
817 Chamber and Thermocouple Psychrometer. 4th European Conference on Unsaturated
818 Soils (E-UNSAT 2020). Lisboa, Portugal, October 19-21, 2020. DOI:
819 <https://doi.org/10.1051/e3sconf/202019503014>

820 Dainese, R. & Tarantino, A., 2020. Measurement of plant xylem water pressure using the
821 High-Capacity Tensiometer and implications on the modelling of soil-atmosphere
822 interaction. *Geotechnique*, <https://doi.org/10.1680/jgeot.19.P.153>

823 Dainese, R. (2020). The use of the high-capacity tensiometer as part of an integrated
824 system to monitor the soil –plant continuum for geotechnical applications. PhD
825 dissertation, University of Strathclyde, Glasgow, UK.

826 Dainese, R., Tedeschi, G., Lamarque, L., Delzon, S., Fourcaud, T., Tarantino, A. (2020b).
827 Cross-validation of High-Capacity Tensiometer and Thermocouple Psychrometer for
828 continuous monitoring of xylem water potential. Under review.

829 Deakin, N. (2005). Repair of subsidence damage: An insurer's perspective. *Journal of*
830 *Building Appraisal*. 1(3): 225-243. DOI: 10.1057/palgrave.jba.2940020.

831 Dean, T. J., Bell, J. P., & Baty, A. J. B. (1987). Soil moisture measurement by an improved
832 capacitance technique, Part I. Sensor design and performance. *Journal of*
833 *Hydrology*, 93(1-2), 67-78.

834 Dias A.S.R.A. (2019). The Effect of Vegetation on Slope Stability of Shallow Pyroclastic
835 Soil Covers. Ph.D. thesis, Naples, University of Naples Federico II, University of
836 Montpellier. <https://tel.archives-ouvertes.fr/tel-02045922>

837 Dixon, M. A., and Downey, A. (2015). PSY1 Stem Psychrometer Manual Ver. 4.4. ICT
838 International Pty Ltd, Armidale, Australia

839 Dixon, M. A., and M. T. Tyree (1984). A new stem hygrometer, corrected for temperature-
840 gradients and calibrated against the pressure bomb, *Plant Cell Environ.*, 7(9), 693–
841 697.

842 Dolidon, N., Hofer, T., Jansky, L. and Sidle, R. (2009). Watershed and Forest
843 Management for Landslide Risk Reduction. In *Landslides - Disaster Risk Reduction*,
844 633-649. DOI: 10.1007/978-3-540-69970-5_33.

845 Fan, J., Scheuermann, A., Guyot, A., Baumgartl, T., Lockington, D. A., 2015. Quantifying
846 spatiotemporal dynamics of root-zone soil water in a mixed forest on subtropical
847 coastal sand dune using surface ERT and spatial TDR. *Journal of Hydrology*, 523,
848 pp. 475-488

849 Gladin, J., 2018. Development of miniature ERT to characterise hillslope subsurface water
850 flow and its interplay with shallow landslides mechanisms. MSc dissertation,
851 University of Strathclyde, Glasgow, UK.

852 Gonzalez-Ollauri, A. & Mickovski S.B. (2017). Hydrological effect of vegetation against
853 rainfall-induced landslides. *Journal of Hydrology*, 549: 374-387.

854 Hillel, D. (1980). *Applications of soil physics*. London: Academic Press

855 Leão, T.P. & Perfect, E. & Tyner, John. (2015). Evaluation of Lichtenecker's mixing
856 model for predicting effective permittivity of soils at 50 MHz. *Transactions of the*
857 *ASABE*. 58. 83-91. 10.13031/trans.58.10720.

858 Ledieu, J., De Ridder, P., De Clerck, P., & Dautrebande, S. (1986). A method of measuring
859 soil moisture by time-domain reflectometry. *Journal of Hydrology*, 88(3-4), 319-328.

860 Lev-Yadun, S. (2011). Bark. eLS.

861 Lu, P., Urban, L., & Zhao, P. (2004). Granier's thermal dissipation probe (TDP) method
862 for measuring sap flow in trees: theory and practice. *Acta Botanica Sinica-English*
863 *Edition*, 46(6), 631-646.

864 Marinho, F. A. M., Take, W. A. & Tarantino, A., 2008. Measurement of matric suction
865 using tensiometric and axis translation techniques. *Geotechnical and Geological*
866 *Engineering*, 26(6): 615-631.

867 Mary, B., Peruzzo, L., Boaga, J., Schmutz, M., Wu, Y., Hubbard, S. S., Cassiani, G., 2018.
868 Small-scale characterization of vine plant root water uptake via 3-D electrical
869 resistivity tomography and mise-à-la-masse method. *Hydrology and Earth System*
870 *Sciences*, 22 (10), pp. 5427-5444

871 Meron M., Grimes D., Phene C., Davis K. 1987. Pressure chamber procedures for leaf
872 water potential measurements of cotton. *Irrigation Sci.*, 8(3): 215-222.

873 Mihai, A & Gere, A & Curioni, G & Atkins, P & Hayati, F. (2019). Direct measurements
874 of tree root relative permittivity for the aid of GPR forward models and site surveys.
875 *Near Surface Geophysics*. 17. 10.1002/nsg.12043.

876 Pagano, L., Reder, A. & Rianna, G. (2018). The effects of vegetation on the hydrological
877 response of silty volcanic covers. *Canadian Geotechnical Journal*, 56(9): 1261-1277.
878 DOI: 10.1139/cgj-2017-0625.

879 Philip J. (1966). *Plant Water Relations: Some Physical Aspects*. *Annual Review in Plant*
880 *Physiology* 17, 245-268.

881 PMS Instrument (2018). [www.pmsinstrument.com/resources/instrument-operating-](http://www.pmsinstrument.com/resources/instrument-operating-manuals)
882 [manuals](http://www.pmsinstrument.com/resources/instrument-operating-manuals)

883 Pollen, N., Simon, A. & Collison, A. (2004). Advances in Assessing the Mechanical and
884 Hydrologic Effects of Riparian Vegetation on Streambank Stability. *Riparian*
885 *Vegetation and Fluvial Geomorphology*, 8: 125-139. DOI: 10.1029/008WSA10.

886 Salisbury, F.B., Ross, C.W., (1992). Plant Physiology. 4th Edition, Wadsworth Publishing
887 Samouëlian, A., Cousin, I., Tabbagh, A, Bruand, A., Richard, G., 2005. Electrical
888 resistivity survey in soil science: A review. Soil and Tillage Research, 83(2), pp. 173-
889 193

890 Scholander P.F., Hammel H.T. et Bradstreet E.D., 1965. Sap pressure in vascular plants.
891 Science, 148, 339-346

892 Sentek Technologies (2019). Sentek Drill & Drop Soil Moisture Probe Installation
893 Training. <https://www.youtube.com/watch?v=fasI3fnNE4Y> (last verified
894 28.01.2019)

895 Tarantino A., Ridley A.M. and Toll D.G. 2008. Field measurement of suction, water
896 content, and water permeability. Geotechnical and Geological Engineering, 26(6):
897 751-782.

898 Tarantino, A. & Mongiovi, L., 2002. Design and construction of a tentiometer for direct
899 measurement of matric suction. s.l., Recife, pp. 319-324.

900 Tarantino, A. & Mongiovi, L., 2003. Calibration of tensiometer for direct measurement
901 of matric suction. Geotechnique, Volume 53.

902 Tarantino, A., 2004. Panel lecture: direct measurement of soil water tension. pp. 1005-
903 1017.

904 Tedeschi G. (2019). The use of vegetation to stabilise the ground: the problem of the
905 measurement of the plant water potential. MSc dissertation, Université Grenoble
906 Alpes, Grenoble, France.

907 Toll, D.G. and Abedin, Z. and Buma, J. and Cui, Y. and Osman, A. S. and Phoon, K.K.
908 (2012). The impact of changes in the water table and soil moisture on structural
909 stability of buildings and foundation systems: systematic review CEE10-005 (SR90).
910 Technical Report. Collaboration for Environmental Evidence.

911 Topp GC, Davis JL, Annan AP (1980) Electromagnetic determination of soil water
912 content: measurements in coaxial transmission lines. Water Resour Res 16:574–582

913 Turner, Neil & Spurway, RA & Schulze, E. (1984). Comparison of Water Potentials
914 Measured by In Situ Psychrometry and Pressure Chamber in Morphologically
915 Different Species. Plant physiology. 74. 316-9. 10.1104/pp.74.2.316.

916 WMO (2018). Guide to Instruments and Methods of Observation (2018 edition). Volume
917 I – Measurement of Meteorological Variables. World Meteorological Organization,
918 Geneva, Switzerland.

919